Model-based Design and Simulation of a Soft Robotic Gripper for Fabric Material Handling

Bowen Wang (wang1nr@uwindsor.ca)
University of Windsor https://orcid.org/0000-0002-1090-1430
Ruth Jill Urbanic

Research Article

Keywords: Soft Robotics, Fabric Material Handling, Model-Based Design, Finite Element Analysis

Posted Date: February 15th, 2021

DOI: https://doi.org/10.21203/rs.3.rs-225922/v1

Model-based Design and Simulation of a Soft Robotic Gripper for Fabric Material Handling

Bowen Wang [1]
Department of Mechanical & Material Engineering, University of Windsor
401 Sunset Avenue, Windsor, Ontario, N9B 3P4, Canada
wang1nr@uwindsor.ca

Ruth Jill Urbanic
Department of Mechanical & Material Engineering, University of Windsor
401 Sunset Avenue, Windsor, Ontario, N9B 3P4, Canada
jurbanic@uwindsor.ca

ABSTRACT

Fabric and textile materials are widely used in many industrial applications, especially in automotive, aviation, and consumer goods. Currently, there is a lack of automatic solutions for rapid and effective fabric handling operations that can be expanded to various applications, causing economic loss, workplace safety issues, and process bottlenecks. As a bio-inspired novel technology, soft robotic grippers provide new opportunities for the automation of fabric handling tasks. In this research, an elastomer-based tendon-actuated soft gripper for fabric pick and place tasks is developed through a model-based design approach. Based on finite element analysis, the gripper design is simulated, modified, and validated. Multiple design variables and their impacts are studied. Detailed motion patterns of the underactuated structure are obtained. After the design is established, a prototype is fabricated trough additive manufacturing and overmolding processes to physically test the functionality of the gripper and further validate the simulation results.

Keywords: Soft Robotics, Fabric Material Handling, Model-Based Design, Finite Element Analysis

[1] Corresponding author:
Bowen Wang [1]
Department of Mechanical & Material Engineering, University of Windsor
401 Sunset Avenue, Windsor, Ontario, N9B 3P4, Canada
wang1nr@uwindsor.ca

Declaration

Funding

No funding was received for this paper.

Conflicts of interest/Competing interests

The authors confirm that there are no known conflicts of interest associated with this publication and there has been no significant financial support for this work that could have influenced its outcome.

Availability of data and material

The authors confirm that all data and material in this paper are available in the manuscript.

Consent to participate

All authors consent to participate in the work of this paper and its publication.

Consent for publication

All authors consent for the publication of this paper.

1. INTRODUCTION

Fabric and fiber composite materials are widely used in various industrial applications. Taking the automotive industry as an example, the introduction of fibre composite materials provides a great amount of advantages compared to traditional engineering materials, such as higher stiffness, higher strength, and lower vehicle mass. Due to the light-weighting potentials, a higher consumption of carbon fiber will be used within the next 20 years [1]. The optimization and automation of novel composite components manufacturing are essential to these requirements.

Pick and place operations for fabric materials are a major technical challenge in relevant domains. There is a wide variety of technologies applied for fiber-reinforcement composites manufacturing. Figure 1 shows the main stages of composites manufacturing. The processes start with semi-finished fiber or fabric materials. These materials are transferred to the mold, preformed, and processed into the final products. Though accomplished in different ways, all composites manufacturing processes involve four basic steps: impregnation, lay-up, consolidation, and solidification [2]. During impregnation, fibers and resins are mixed to form a lamina in order to make sure that the resin flows entirely around all fibers. In the lay-up step, composite laminates are formed by placing prepregs at desired locations and angles, where the desired composite thickness and shapes are achieved by the number of layers and the structure of moulds. Then, the consolidation step creates intimate contact between each layer to ensure the removal of entrapped air between layers. The

final step is solidification, which may take less than a minute or up to two hours depending on the curing method. The potential of significant mass reduction strategies that can be presented using composite fiber solutions are offset by the high labor intensity and long cycle time. Improvements made to the transferring processes can effectively reduce the total cycle time.

At this time, there is a lack of automatic solution for effective pick and place activities for air-permeable and highly flexible components that can be applied in the composite fiber manufacturing domain. A great portion of the present pick and place operations for flexible components such as fabric mats are performed manually in the industry, causing low production efficiencies, economic losses, and workplace health and safety issues (due to repetitive motion stresses).

Novel breakthrough on soft robotic technologies, e.g. bio-inspired machines that are more flexible than traditional rigid-bodied robotic machines, provide new insights for solutions in this problem domain. Traditional principles applied for fabric material handling include needle piercing, clamping, vacuum, adhesion, etc. Though efficient under some circumstances, all these methods have their own limitations [3]. In comparison, soft robots have bodies made of flexible materials and have a relatively large number of degrees of freedom, making them effective for picking up highly deformable of fragile objects [4]. Hence, they have great potentials to accomplish typical fabric picking tasks by mimicking manual operations. The aim of this research is to develop a gripper for fabric material handling, applying a soft robotics-based technology.

2. Background

2.1. Fabric Materials

Fabrics or textiles are flexible materials constructed by a network of yarns, which are produced by interlocking raw fiber materials. Most fabric materials can be regarded as flat sheets that are flexible and deformable. There are various categories of properties that can be used to describe the performance of fabric components. Based on the methods fabrics are built up from textile fibers, there are various types of fabric structures, such as woven, knitted, braided, etc. Different types of fabric structures have different material properties in terms of stability, drape, porosity, smoothness, balance, symmetry, and crimp.

While performing pick and place tasks using robotic grippers, the most important properties are the fabric structure, roughness, area weight, and stiffness. The roughness can be expressed by the friction coeffect. As for stiffness, a typical parameter is the bending length, which can be calculated by the Peirce's cantilever method [5]. As shown in Figure 2, A strip of fabric of specific size is place on a platform and moved forward until the centerline from the edge of the platform to the leading edge of fabric makes an angle θ to the horizontal plane by self-gravity.

Therefore, the bending length c can be calculated by the cantilever length l and the angle θ:

$$c = l\left(\frac{cos(\theta/2)}{8\tan\theta}\right)^{1/3} \quad (1)$$

Aside from material properties, geometric properties of the fabric pieces such as size, thickness, shape are also important variables. Many processes require to attach fabric mats onto three-dimensional mold surfaces, making the pick and place tasks more complicated.

2.2. Contemporary Handling Solutions

Various approaches for fabric material handling have been investigated in the past.

Early research focusing on gripping technologies for flexible materials started at the end of last century. Several experimental gripping solutions have been developed since the 1990s. Taylor [6] concluded some common gripping systems for flexible materials at the time. By compiling previous research, Koustoumpardis and Aspragathos [3] derived a classification system based on the gripping principles and handling techniques.

The most frequently investigated gripping principles are clamping/pinching and vacuum-based solutions. Some traditional grippers applied simple mechanism to pick up fabric components. These solutions usually have problems on dealing with slippage and wrinkling/folding during pick and place operations [7,8]. A series of studies have presented a gripper that combines vertical picking and side picking approaches and operates as a human hand [9,10]. It is a complex mechanism with multiple degrees of freedom (DOF). Vacuum grippers cause minimal harm or distortion to the fabric materials. Kolluru et al. [11] have developed a vacuum gripper that has a flat bottom surface constituting a matrix of holes for suction purposes. A variety of modified

configurations have been developed based on it, with intelligent control integrated [12,13]. The biggest limitation for a vacuum gripper is due to the air permeability of fabric materials. Vacuum systems are also complex and expensive. Other strategies like pinning or adhesive grippers have also been developed, but their applications are limited due to the damage to the fabrics or remaining adhesive materials on the gripping surface.

New types of grippers have been developed independently or based on existing grippers modified. One typical approach is the integration of sensors to increase the material handling efficiency [14-16]. Much recent research is based on the vacuum strategy. Costo, et al. [17] have developed a gripper frame with three vacuum end effectors. Kordi et al. [18] have developed a more complex configuration with eight movable vacuum end effectors arrange on a flexible frame. Ragunathan and Karunamoorthy [19] have done a similar design with four end effectors. Research done by Flixeder et al. [20] has integrated a de-wrinkling roller on a Coanda-effect gripper frame. These solutions can deal with complex fabric geometry, but they still have the previously mentioned limitations of vacuum-based grippers.

Although not common, clamping grippers with soft robotic features have been studied for some specific cases. Doulgeri and Fahantidis [21] developed a rigid robotic gripper with soft-tipped fingers to pick up fabric material pieces while avoiding slippage and damage. Murakami and Hasegawa [22] have presented a gripper with a human-like fingertip and a complex mechanism. Koustoumpardis et al. [23] performed a research

on an underactuated robotic gripper that can successfully grasp, transfer, and de-wrinkle for simple fabric materials.

As a foundation of this paper, previous research has shown that with the introduction of compliant structures, it is possible to reliably pick and place fabric materials without introducing slippage or damage [24]. The wrinkling and distortion of the fabric ply after placing can be avoided through appropriate toolpath planning [25]. Though the proof of concept was validated with a simple gripper in the research, a more flexible design would be needed to deal more realistic scenarios, e. g., picking from curved surfaces.

2.3. Soft Robotic Grippers

The application of soft robotic grippers in fabric handling tasks has two important advantages. Since soft robotic grippers are mostly underactuated, they can automatically adjust to the geometry of the objects to be picked. Therefore, the complexity of the geometric shapes of fabric materials would not be a challenge during picking. An underactuated gripper has the potential to pick up deformable fabric materials from curved or inclined surfaces and perform certain processing with relatively complex gestures. Secondly, those grippers usually have contact surfaces made from soft and deformable materials such as rubbers or soft plastic, which can provide a firm gripping condition while not damaging the fabric material.

Soft robotic technology and underactuated grippers have been widely studied during past decades. Birglen, et al. [26] have presented a comprehensive review on underactuated gripper hands. Kim et al. [27] did a similar review upon bio-inspired soft

robotics. More recently, Shintake, et al. [28] have carried out a through introduction of soft robotic technology that covered most of the temporary soft robotic grippers. These papers have also discussed the fabrication and control strategies for soft robotic grippers.

The most common soft robotic gripper configuration is based on compliant structures being deformed by external or integrated actuators. Objects can hence be gripped through impactive prehension. There are various ways of actuation that have been studied by researchers.

As traditional rigid grippers can be driven by rotary of linear motions, one efficient way to achieve actuation force for soft gripers is to drive passive structures by external motors. Based on the location of the actuation, the working principles can be distinguished as contact-driving deformation and tendon actuation. For contact-driving deformation grippers, the actuator only drives the finger to linearly enclose such as rigid grippers, and the gripper material adjusts to the target object by passive deformation. The tendon-driven grippers have driving cables embedded inside the gripper structure to transmit the actuation force. These grippers are mostly made by articulate elastomer fingers connected to a rigid palm. The fingers can also be hinge-connected linkages confined by elastomer skin or other elastic components.

Another popular design for actuation is to apply pneumatic or hydraulic power [29,30]. Fluidic elastomer actuators, also known as soft pneumatic actuators, are one of the oldest designs for soft robotics, yet they are still widely applied in both academic studies and industrial applications. The actuation is achieved by feeding gaseous or

liquid fluid into a chamber made of highly elastic materials. The inflation of the chamber then bends the gripping structure, which is usually asymmetrical or uses anisotropic materials. These grippers usually have a large bending capacity. The actuation time may vary drastically based on the details of the designs.

Some characteristics of these mentioned configurations are summarized and compared in Table 1.

To actuate passive structures, there are many other novel approaches as well, including dielectric elastomer actuators, ionic polymer-metal composites, shape memory materials, etc. Aside from actuating passive structures, soft and adjustable gripping can also be achieved by varying the stiffness of the gripping structure. These approaches do not fit the purpose of this research and will not be discussed further.

3. Methodology

There are three important characteristics of fabric materials to consider for handling operations: their light weight, high deformability, and complex geometry. Compared to other objects manipulated in industry, common fabric materials such as carbon fiber fabric or glass fiber fabric have much lighter density, making them easier to carry. Hence, the demand for the gripping force is necessary but not very high. Conversely, their smooth surfaces may require a higher gripping force to prevent slippage during transfer activities, which will lead to fiber damage. Fabric materials are highly deformable, causing draping and shifting during the pick and place operations. Deformability also causes many types of fabrics vulnerable to hard contact, making

grasping more challenging. The geometrical complexity is related to various mold shapes used in industry. During the application, the gripper might need to pick or place fabric plies with respect to curved or cornered surfaces. Deformation of the fabrics also increases the geometrical complexity. Aside from these three characteristics, efficiency and motion speed are also required as for any other pick and place operations.

Although traditional grippers might be able to perform fabric picking operations under limited scenarios as past literature suggests, they can hardly remain feasible to deal with the increasing complexity in many applications. Previous research mentioned in literature review proved that compliant structure can be applied for simple fabric handling tasks, but complex scenarios require more flexible gripper designs [25].

3.1. Working Principle

Many fabric handling operations are performed manually. To develop a soft gripper adjustable to various scenarios, the motion of human hands is evaluated. When manually picking up a ply of fabric, the index finger and thumb are typically applied. As shown in Figure 3, at the beginning of the picking movement, the index finger and the thumb open wide so that the finger pulps become parallel the fabric surface. Then, the finger pulps are pushed toward the fabric to create a firm contact condition. While picking up, the hand would lift upward whiling pinching the fabric up through friction force. After the movement is finished, the fabric would be firmly clamped between the two fingers.

According to the literature review, finger-based gripper designs with cable actuation appear to be the most suitable configuration for fabric handling tasks because

of their high actuation speed, steady and reliable gripping force, and structural simplicity. They are capable of rapid movements, providing firm gripping condition, and complex gestures for various operations. This type of gripper is also compatible with novel grasping, smoothing, and de-wrinkling strategies. A fluidic elastomer actuator is another competitive candidate, as they also provide high gripping capability, but are not favored due to their mechanical complexity and relatively lower actuation speed.

For the purposes of this research, it is required that the gripper should have a large and controllable opening magnitude. It should be able to adjust itself to the working surface when engaging picking or placing motions while providing enough gripping force. When fully enclosed, there should be enough contact area between the fabric and the gripper tip to prevent slippage. That means the gripping fingers should be able to bend in double directions and the bending magnitude being controlled by a simple input, which is the pulling force for cable actuation. A typical cable actuated gripper configuration is based on elastomer fingers with gaps on the bending sides and driving tendons inserted through the gaps. To achieve controllable double-direction bending, there should be gaps on both sides of the finger. Figure 4 illustrates a conceptual version of such design.

As shown in the drawing, multiple triangular apertures are distributed on the bending side of the finger, separating the elastomer bar into multiple sections. Two slots are present at the gapped edge for the driving tendons to go through. At the top section, there are U-shaped slots strengthened by a stiffer material to hold the tendons. These underactuated fingers would be attached to a rigid ‘palm’ structure. When the

driving force pulls the tendons from the bottom, the gripper would open or enclose due to the pulled sides. When touching the working surface while enclosing, the gesture of the fingers would be confined by its elasticity behavior, hence adjusting itself to the target geometry. Figure 5 illustrates the resting, opening, and gripping positions of a conceptual gripper configuration. The potential for complex gestures also allows flexible touching areas for various gripping and smoothening requirements.

3.2. Material Models

Compared to the computational analysis of traditional rigid body systems, design and simulation tools are limited for soft materials, including fabrics and elastomer materials that are essential for soft robot grippers. While the position and movement of rigid objects can be sufficiently described by six degrees of freedom (three transitional coordinates and three rotational coordinates), soft bodies cannot be confined to simple and discrete planar motions. Soft materials are elastic and can be highly bent, twisted, stretched, compressed wrinkled, etc. Therefore, the analysis and simulation for soft bodies are much more complicated than rigid bodies.

In order to analyze the performance of soft grippers and fabrics, special analysis approaches such as Finite Element Analysis (FEA) are applied. Various studies have applied FEA simulation among those subjects. The simulation challenges also require sophisticated modelling of the structural and dynamic configurations of the system, which will be discussed in the next section. Abaqus is used to perform the simulation. This allows the model-based design of the gripper configurations.

3.2.1 Simulation of the Underactuated Mechanism

The most critical part regarding the simulation of soft robotic grippers is the modelling of the elastomer fingers and similar structures. For this task, hyperelastic material models are necessary to capture the nonlinear material properties of the rubber-like materials.

For rubber-like materials such as elastomers or bio tissues, a large strain occurs when a small stress is applied. Traditional linear theories of elasticity represented by Hooke's law fail to adequately predict their mechanical behaviors. During the past decades, researchers represented by Mooney and Rivlin have introduced a nonlinear theory of elasticity that leads to hyperelastic material models using strain-energy functions to describe the mechanical properties of rubber-like materials [31-33]. Specifically, hyperelastic models are ideal for characterizing silicone rubber materials in industrial applications [34,35].

In the hyperelastic theory, the materials are assumed to be isotropic and incompressible. This is generally valid for rubber-like materials, especially when they are not strictly confined. A hyperelastic material model relies on the strain-energy function Ψ, which is obtained from symmetry, thermodynamic and energetic considerations.

If the material is isotropic, the strain-energy function depends on the strain invariants. That is

$$\Psi_{isotropic} = \Psi(I_1, I_2, I_3) \tag{2}$$

where the strain invariants

$$I_1 = \sum_{i=1}^{3} \lambda_i^2 \tag{3}$$

$$I_2 = \sum_{i,j=1}^{3} \lambda_i^2 \lambda_j^2 \, , i \neq j \tag{4}$$

$$I_3 = \prod_{i=1}^{3} \lambda_i^2 \tag{5}$$

λ_1, λ_2, and λ_3 are the principle stretches [35].

If given the assumption that the material is incompressible ($I_3 = 1$), Equation 2 becomes

$$\Psi_I = \Psi(I_1, I_2) \tag{6}$$

Since the strain invariants directly depend on the principal stretches as mentioned in Equations 3 to 5, the strain-energy functions can also be expressed as a function of the principle stretches:

$$\Psi_I = \Psi(\lambda_1, \lambda_2, \lambda_3) \tag{7}$$

In the more complicated cases such as biomechanics where anisotropic characteristics are present, an anisotropic contribution can be added to compensate for the anisotropic nature of those materials. Hence, the full expression of Ψ becomes

$$\Psi = \Psi_{isotropic} + \Psi_{anisotropic} \tag{8}$$

An example of such cases is the Martins material model. However, such complicated cases are not within the domain of this paper.

Multiple models have been established by researchers, such as the Neo-Hookean material model, the Mooney–Rivlin material model, the Yeoh material model, the Ogden material model, etc. The majority of these models are based on one or more

quantities among the principle stretches λ_1, λ_2, λ_3 and the Cauchy–Green tensor invariants I_1, I_2, I_3. The four mentioned models are all available in the Abaqus software.

Relevant studies have shown that in cases where the deformations are moderate (<100%), simple models like the Neo-Hookean model would suffice; the Mooney Rivlin model potentially remains accurate until the deformations reach approximately 200%. The Yeoh model and the Ogden model can provide accurate results under large deformations, but the complexity of these models leads to high computational costs [34,36].

In the study of soft robotic grippers, the deformations of the elastomer materials are significantly smaller than the capacities of the simpler models mentioned above. Therefore, by balancing the accuracy and computational efficiency, the Mooney-Rivlin was initially selected as the hyperelastic model for elastomer materials in the research. It is one of the earliest developed hyperelastic models and is well known for its high accuracy in describing the mechanical behaviors of isotropic rubber-like materials. The strain-energy is expressed as

$$\Psi = c_1(I_1 - 3) - c_2(I_2 - 3) \tag{9}$$

The elastomer material used for prototyping in this research is Mold Star 15 SLOW silicone rubber. There were no data regarding hyperelastic models readily available. Thus, a tension experiment was designed and performed to obtain the Mooney-Rivlin coefficients c_1 and c_2.

The uniaxial tensile test followed the ISO 572-2 standard. A dumbbell-shape sample was designed as shown in Figure 6.

During the test, the sample underwent an increasing uniaxial load until the deformation reached 100%. The test was performed with unfixed tension gauge, so the deviation was high. In order to ensure the validity, the test was performed multiple times. After the data was collected. The coefficients c_1 and c_2 were obtained using the curve fitting toolbox in MATLAB. The results were $c_1 = 0.08412$ and $c_2 = -0.04687$. Figure 7 shows the fitting result compared with the experimental data.

The SSE was 0.005717. The R-squared was 0.9878. The adjusted R-squared was 0.9874. The RMSE was 0.01429. According to the figure, there was good fit between the material model and the experimental data. However, when the stretched a certain level in the compression region, this model predicted unrealistic behaviors. This could lead to convergence problems during simulations.

A suggested way to solve this problem is to force c_2 to be positive [37]. With this extra constraint introduced, the result became $c_1 = 0.05773$ and $c_2 = 0$. The material model hence became identical to a Neo-Hookean model. Figure 8 shows the adjusted fitting result.

The squared estimate of errors (SSE) is 0.01141. The coefficient of determination R-squared is 0.9757. The adjusted R-squared is 0.9749. The root-mean-square error (RMSE) is 0.02019. Though the fitting goodness is slightly lower than the first model, this model remained accurate.

Based on these results, a finite element (FE) model of the test sample is established in Abaqus, as shown in Figure 9. The quality of an FE model can be evaluated

by the correlation coefficients (CC) between experimental and simulation data, which can be given by:

$$Correl(X,Y) = \frac{\sum(x-\bar{x})(y-\bar{y})}{\sqrt{\sum(x-\bar{x})^2(y-\bar{y})^2}} \quad (10)$$

where *X* and *Y* are the experimental and simulation data respectively. $\bar{x}$ and $\bar{y}$ are the average of corresponding data.

Figure 10 shows the comparison between FEA result and the test data that validated the material model. The CC of this model was 0.9896, proving its validity.

3.2.2 Simulation of Fabric Materials

These results indicate that the gripper design can be virtually tested. To do so, a material model that can characterize the basic behavior of fabric plies during pick and place operations is necessary.

The simulation of fabric materials under large deformation is a challenging problem in relevant research. In Abaqus, the “lamina” type of elasticity is available for describing the orthotropic behaviors of fabric materials. This elastic model is characterized by six parameters: Young’s modulus E1 and E2, Poisson’s ratio v12, and shear modulus G12, G13, G23. Researchers have also developed algorithms and subroutines to accurately capture the anisotropic behaviors of fabric by modelling the microscopic interaction between each yarn that constitutes the fabric ply [38-40].

Though proved reliable to simulate the deformation of fabric materials with high accuracy, these methods have high computational expenses. As the purpose of fabric simulation is to verify the capability of the gripper design to pick up fabric materials, the

accurate stress and strain distributions of the fabrics are not needed. Therefore, it would be possible to model the fabric as an isotropic ply, where only two parameters (Young's modulus E and Poisson's ratio ν) are needed. Researchers have applied such simplified approach for simulating the wrinkling and draping behaviors of flexible fabric plies and other laminae [41].

As mentioned in section 2.1, the most important properties of fabric materials during gripping motions are the roughness and stiffness. While roughness can be simply characterized by the coefficient of friction, stiffness should be calibrated based on experimental draping behavior. The fabric sample used in this research is plain woven carbon fiber fabric. The thickness of the fabric ply is 0.2 mm. The density is 1.15×10^{-3} g/mm^3.

A cantilever experiment is performed following the method described in section 2.1. As demonstrated in Figure 2, a 5 cm wide strip of the fabric is placed on a platform and moved forward until the centerline from the edge of the platform to the leading edge of fabric makes a 41.5° angle to the horizontal plane. The bending length c is measured to be 4.28 cm. The length l of the hanged section of the fabric strip before bending is 8.40 cm.

In order to ensure the validity of the isotopic FE model, an equivalent pair of parameters should be found so that the model would result in the same bending length. A 50 mm by 84 mm rectangular shell part is modelled in Abaqus and meshed using S4R elements. A 9800 N/ton gravity field is applied. The encastre boundary condition is applied to one short edge of the ply to simulate its bending under self-weight as the end

section of a long flat strip. It is found that with the equivalent parameters E set to 240 MPa and v set to 0.1, the simulation result (shown in Figure 11) shows the same draping behavior as the experiment.

3.3. Simulation Models

Applying the material model developed in the previous section, it is feasible to perform the model-based design (MDB) of the soft gripper in Abaqus.

The gripper design is based on the conceptual configuration shown in Figure 4, where the angle of each gap is 60 degrees and the depth of the gap is 6 mm. A 1 mm fillet was designed at the inner vertex of the gap to prevent stress concentrations. The distance between two adjacent gaps is 15 mm. The width of the finger is 25 mm. Other features and their effects on the mechanical behaviour need to be analyzed using FEA simulation. The main design variables include the finger thickness (the distance between the two gaped sides) and the number of gaps distributed on each side.

Since the structure of the elastomer finger contains a linear pattern, the mechanical behavior of the whole finger is based on that of each section. For each section, the bending magnitude of caused by a fully enclosed gap is related to the thickness of the finger. An FE model is established to simulate the behavior of a single section, as shown in Figure 12.

Because the structure is symmetrical, only half of the section need to be modeled. Symmetrical boundary conditions for the Z-axis is applied to the corresponding surface. A contact relationship is established between the slot and the string surfaces. Self-contact is established on the gaped surface. This simulation is a

static simulation, for this simulation focuses on the mechanical behavior under relative static conditions rather than its dynamic responses. Due to the same reason, the friction between the contact pairs can be neglected.

An encastre boundary condition is applied to the bottom surface of the finger to fix it to the ground. The top surface is coupling constrained to the same control point as the upper tip of the driving string. Therefore, when the string is pulled downward, the entire top surface would rotate as a plain surface, which is the same as the behaviour of a section when the whole finger bent. The bending magnitude of one section φ_i equals to the angle between the top surface and the horizontal plane.

The hyperelastic material model developed in section 3.5 is applied for the elastomer body, while the string was modelled using elastic material. The model is segmented and meshed using C3D8RH elements. The string is meshed using C3D8R elements. A 4.8 mm displacement is applied to the bottom tip of the string. the maximal bending magnitude of the top surface is recorded. The driving force, which is the reaction force at the bottom tip of the string, is recorded as well. The simulation is run with different finger thickness.

When the maximal bending magnitude of a single section φ_i is known, the maximal bending magnitude of the whole finger can be given by

$$\varphi = \sum_{1}^{n} \varphi_i \tag{11}$$

where n is the number of gaps on the corresponding side.

After the finger thickness is determined, a full FE model of the finger can be developed to investigate the effect of the distribution of gaps, as shown in Figure 13a.

Like the one-section model, this model is symmetrical along the Z-axis. Contact pairs are established. The coupling constraint is applied to the inner surface of the U-shaped tube to connect the finger and the string. The coupling constraints limite all six degrees of freedom, causing the relative position of every node on the constrained surface to remain constant to the control point. Compared to the physical finger where the U-tube may slightly deform, this simplification is not 100% realistic. However, the detailed stress and deformation on the U-tube, which is much more rigid the silicone rubber, are not of concern. Therefore, such simplification is acceptable.

The finger model is sectioned and meshed mainly with C3D8RH hexahedral elements. Due to the geometrical complexity, C3D4H tetrahedral elements are used at the regions where the U-shape tubes are present. Being a linear element, C3D4H does not have high integrity during analysis, but this problem can be neglected for the detailed behaviors in those regions are not of concern. The mesh around the regions where contact or large deformation would happen are created denser. The string is still meshed using C3D8R elements. Figure 13b shows the meshing strategy.

By changing the number of the gaps on the outer side or the inner side, there could be several variations of the finger model. A combination of outer and inner gaps can be represented by an abbreviation code OxIy, where a number x stands for the number of gaps on the outer side and a number y stands for the number of gaps on the inner sides. The configuration in Figure 13 can be noted as O3I3. In this research, the simulated configurations include O2I2, O3I1, O3I2, O3I3, and O4I4. For each

configuration, a 4 N force is applied downward at the bottom tip of the string. The displacement of the bottom tip of the string and the driving force are recorded.

A similar model can be used to simulate the gripping movements, as shown in Figure 14. An analytical rigid plane is fixed at the midplane of the gripper where the gripping would happen. The finger and the string are constrained and meshed using the same strategy. A 6 N driving force is applied, and the gripping force occurred on the midplane is recorded.

At last, the gripper design can be finalized based on the analysis results. A dynamic explicit simulation would be established to verify the functionality of the gripper, where the material model of the fabric ply developed in section 3.2.2 is applied as the workpiece.

3.4. Prototyping

Selected additive manufacturing (AM) and other related processes are utilized for prototyping.

Additive manufacturing includes various processes that create three-dimensional objects by joining materials directly from a digital model. In this research, the AM technology utilized is the fused deposition modeling (FDM) process, where a physical object is created directly from a CAD model using layer-by-layer deposition of a feedstock plastic filament material extruded through a nozzle. Rigid components can be directly created through FDM processes, while elastomer components can be molded using 3D printed mold sets.

Another important prototyping technique used in this research is the overmolding process. Overmolding is a molding technique where two or more different materials are combined together to create a single part. Typically, during overmolding, the substrate materials are partially or fully covered by subsequent materials referred as overmold materials. The substrate materials are usually more rigid than the raw subsequent materials before curing. These processes include plastic over metal molding, rubber over plastic molding, rubber over metal molding, rubber over plastic molding, etc. Overmolding processes can be used to fabricate complex structures with multiple materials included.

Taking the elastomer finger in Figure 4 as an example (three-gap version), the part can be overmolded using a mold set with movable components. The plastic U-shape tube is the substrate material, and silicone rubber is the subsequent material. As illustrated in Figure 15 (only half of the mold set is shown here), the basic geometry of the gapped elastomer finger can be directly created from the mold shape, and two removable tubes are inserted into the cavity to create the cable slot. The U-shape tube is held by the extractable tubes. After the subsequent material cures, the extractable tubes would be removed, leaving the U-shape tube inside the elastomer structure as part of the finger.

The FDM machine used in this research is a Fortus 400mc 3D printer. ULT9085 is used to make rigid components. UTL_S is used as support material when there are complex geometries or overhang angles that exceed the threshold (approximately 45° depending on material types and extrusion characteristics). The elastomer material used

in this research is Mold Star 15 SLOW silicone rubber, a mediate hard, strong rubber material that is tear resistant and exhibits very low long-term shrinkage.

4. Results and Discussion

The simulation is performed to determine the final soft gripper design. Once this is obtained, prototyping occurred.

4.1. Simulation Results

4.1.1 Investigation on Finger thickness

Two typical results are shown in Figure 16 as examples. When the 4.8 mm displacement was accomplished, the gap became fully enclosed, and the top surface rotated to a certain degree. After the result was obtained, the model was re-meshed denser to test its validity. As the mesh was refined, the change of result was less than 5%, proving the appropriateness of the FE model.

Figure 17 shows the relationship between the maximal bending magnitude and the finger thickness. Figure 18 shows the relationship between the maximal driving force and the finger thickness.

According to the results, as the thickness of finger increases, the maximal bending magnitude decreases, and the driving force increases. Usually, larger bending magnitude and smaller driving force are preferred. However, when the thickness is too small, the stiffness of the finger would become too small, hence make it less controllable and unreliable. The actual thickness should be decided based on the size of

the gripper. In this research, the thickness is chosen to be 20 mm, where the maximal bending magnitude is close to 30 degrees.

4.1.2 Investigation on Gap Distribution

The simulated configurations include O2I2, O3I1, O3I2, O3I3, and O4I4. For each configuration, a 4 N force is applied downward on the bottom tip of the string. Figure 19 shows the bending results. Figure 20 shows the displacement-force relationships for different configurations.

The actuation cannot reach its full capacity for some cases due to convergence difficulty, but the trend is available. It can be observed that when the gap distribution is symmetrical, more gaps/sections lead to lower stiffness. That is, less force is required for the finger to bend to a certain magnitude. When the number of gaps remains constant on the outer side, decreasing the number of gaps on the inner side increases the stiffness.

If the stiffness is too high, not only too much actuation force would be required, but the maximal bending magnitude would not be able to reach 90°, as in the cases of O2I2 and O3I1. Extremely low stiffness is not desired, either, for the finger would become less controllable and highly sensitive to environmental disturbances. A typical example is the draping under gravity. When the gripper is aligned parallel to the ground, the maximal vertical displacement at the tip caused by self-weight is 5.97 mm for the O3I3 configuration and 14.14 mm for the O4I4 configuration.

4.1.3 Investigation on Gripping Behavior

It is discovered that when there are too many gaps on the inner side, the gripper would bend around multiple gaps, causing the tip to roll against the gripping plane, as shown in Figure 21a. The bending continued as the upper gaps enclosed and the bottom gap opened up. This rolling grip phenomenon would cause poor contact condition and is not desired. This problem can be solved by limiting the number of gaps on the inner side. As for the O3I2 configuration shown in Figure 21b, the rolling grip stopped as the upper gap fully enclosed. The elastic nature of the elastomer material would then create firm gripping that can adjust to the shape of the object to be gripped.

It is also discovered that the distance from the midplane to the fingertip does not affect the gripping efficiency, which is the ratio of the gripping force to the driving force. Meanwhile, by adding an inclined surface at the fingertip, as shown in Figure 22, the gripping efficiency can be increased.

Different fingertip angles are simulated and compared. Figure 23 shows the relation between the gripping force and the driving force under multiple scenarios.

At the beginning of actuation, the gripping force remained zero until the fingertip touched the midplane. The gripping force then started to increase proportionally with the driving force. A larger tip angle leads to higher gripping efficiency, but this advantage become less significant as the tip angle increases. A larger tip angle would also increase the size of the gripper and make it more sensitive to gravity. The actual parameter should be decided based on the application.

4.1.4 Final Design and Gripping Simulation

Balancing all previously mentioned variables, the final design is an O3I2 configuration with 20 mm finger thickness and a 15° fingertip. Figure 24 shows the CAD design of the gripper assembly.

Based on the geometrical symmetry of the gripper design, the behavior of the full gripper can be obtained from the half-finger FE model (force multiplied by four). Because the TCP would shift as the fingers bend, the deformation of the fingers during the opening movement would be important reference data for control. As shown in Figure 25, a reference point is created from the extension lines of the geometrical boundaries of the fingertip to monitor the tip displacement during the opening process.

The relationship between the string tip displacement and the driving force is shown in Figure 26. Figure 27 shows the relationship between the fingertip displacement on vertical direction and the driving force. And Figure 28 shows the trajectory of the tip reference point for one finger (using the initial position as the origin).

A dynamic explicit simulation is established to verify the functionality of the gripper design, as shown in Figure 29. Two fingers are located symmetrically in respect of the Y-Z plane. An analytical rigid plane that serves as the working surface is placed underneath. The fabric workpiece is modelled to be a 300 mm by 100 mm rectangle and is place on the rigid plane. Due to the geometrical symmetry, the model includes only half of the physical scenario. A symmetrical boundary condition among Z-axis is applied to the corresponding side of the fingers and the fabric ply.

The complexity of this model is much higher than the simulation of a single finger. Multiple simplification strategies are applied to save the computational expense. Since the accurate force-deformation relation of the elastomer finger is no longer of concern, the models of the actuation cables and slots are removed. Instead, the actuation is achieved by applying forces onto certain reference points that are coupling constrained with certain geometry on the finger models. The forces are adjusted so that the finger deforms in a nearly identical way as the realistic model previously studied.

The simulation includes three steps: opening, gripping, and lifting. The bottom surfaces of the two fingers are fixed at all time. Meanwhile, the rigid plane moves steadily to relatively simulate the lifting and lowering movements of the gripper during the picking operation. According to experimental data, the friction coefficient between the fabric and the working surface is set to 0.3. The friction coefficient between the fabric and the fingertip is set to 0.7. Other contact pairs are simplified as frictionless. A 9800 N/ton gravity field is applied. At the opening stage, the rigid plane moves upward for 35 mm as the fingers bend to open the gripper. At the gripping stage, the rigid plane steadily moves back to its original position, and the modified loading condition causes the gripper to enclose and grip the fabric. Finally, the rigid plane moves downward, causing the fabric to be picked away from the working surface.

Figure 30 shows the complete picking process for the simulation result. The visualization of the result is mirrored in respect to the X-Y plane. It is thus verified that the gripper can successfully pick up the fabric ply and hold it firmly, as the design criteria requires.

Similarly, a modified FE model shows that the gripper can also pick up the fabric ply from a curved surface, as shown in Figure 31.

4.2. Prototyping and Experiment

A prototype is fabricated using the methods mentioned in section 3.4. Based on the CAD model, a mold set is created through FDM process. The mold set is shown in Figure 32a.

Figure 32b shows the assemble strategy for overmolding. The heat-shrink plastic tube is soft when heated so it can be deformed to create the U-shape permanent tube. The rigidity of the tubes becomes much higher after fully shrank and cooled down. Two extractable tubes, on which the U-shape tube are attached, are inserted through pre-built holes on the mold. After the silicone cures, the sticks would be removed, and the U-shape tube remaines inside the finger. The driving string would then go through the U-shaper tube and the slot in the finger that was formed by the extractable tubes.

The gripper base are also directly printed though FDM process. Figure 33 shows an assembled gripper prototype (without driving mechanism).

It takes 2 hours and 35 minutes to print the mold set and approximately 3 hours to remove the support material. The material used to make the mold set is ULT9085. The time and effort spent on removing support material may be reduced if the AM material is polycarbonate or ABS, as the support material can be removed more easily and thoroughly. With the mold set prepared, it would take about an hour to mold one silicone finger. The gripper base takes an hour and 26 minutes to print and

approximately 30 minutes to remove the support material. The time consumption is summarized in Table 2.

As so calculated, it would take approximately 3 hours and 56 minutes to make one gripper prototype with the mold set available, which is quite efficient.

The weight of one finger is 51 g. the weight of an assembled gripper is 127.5 g. The geometrical are measured. A bluing test (using Prussian blue ink) is performed to observe the contact condition. Table 3 summarizes these geometrical data of the gripper prototype.

Because the access to change the robot gripper cannot be obtained during the research period due to COVID-19, a manual test is performed to verify the capability of the gripper. The tests include picking up a single fabric ply, separating one ply from a stack, and the de-wrinkling process. It should be noticed that the human operations during the tests only include pulling the actuation tendons and pressing the gripper base linearly, so the processes can be easily programmed with a robot.

The opening magnitude of the gripper can be controlled by the actuation force, so is the bending angle of both fingers. The gripping interaction is a result of the friction between the fingertip and the fabric ply, which can be achieved by applying a pressure perpendicular to the working surface. With the large variety of opening gestures, the gripper can obtain a firm gripping from inclined or curved surfaces. It is also shown possible to separate one fabric ply from a stack of fabric mats. By applying a moderate pressure perpendicular to the fabric surface while gripping, the gripper can successfully pick up a single ply without causing any disturbance to the fabric underneath. Finally,

the gripper can also be used for de-wrinkling by reversing the gripping motion. These processes are shown in Figure 34.

The force response during the actuation procedures are measured using a force gauge. Figure 35 shows the relation between the displacement of the string tip the driving force. The data is compared with the simulation data previously obtained to validate the FEA results.

The CC of the experimental data and the simulation data is 0.9882. The simulation successfully predicted the overall behaviour of the gripper. It can be observed that there is relatively larger error at the initial stage, where the experimental data shows an accelerating trend that the simulation does not capture. This may be caused by imperfection of the hyperelastic material model used in the simulation. Other factors may also accumulate to the error, such as the shift between the U-shape tube and the inner surface of the elastomer, the elastic behavior of the string, the measurement error, etc.

5. Summary and Conclusions

In this research, an elastomer-based soft robotic gripper for fabric handling tasks is designed using an MBD approach with FEA simulations. The gripper is tested through both simulation and prototyping.

It is confirmed that a tendon actuated soft gripper that mimics the motion of a human hand can be applied to perform fabric pick and place operations effectively under various scenarios. The thickness of the elastomer finger and the distribution of

gaps on the finger structure both affect the behavior of the gripper. Though appropriate structural design, controllable finger motions and firm gripping conditions can be achieved.

The new technologies used here show great potentiality for relevant research. FEA simulation is a crucial tool for the design of soft robotic grippers. The behavior of underactuated mechanism and flexible materials, which are essential features of soft robotic grippers and cannot be described analytically, but they can be studied and predicted with high accuracy through FEA simulation. It can also be used to simulate fabric materials to validate the functionality of a gripper design. AM and overmolding processes are useful technologies for prototyping and experiments. Once a design is finalized by simulation, a prototype can be fabricated through these processes in a very short time.

For the future work, the simulation model can be further improved to make it more accurate and realistic. More design variations can be explored, and sensor embedded in the gripper fingers. The control strategies of the gripper design should be designed using force data for feedback and tested.

NOMENCLATURE

DOF	degrees of freedom
c	bending length
l	cantilever length
ϑ	cantilever angle
MBD	model-based design
FEA	finite element analysis
FE	finite element
Ψ	strain-energy
I_i	strain invariant
λ_i	principle stretch
c_n	Mooney-Rivlin coefficient
SSE	sum of squared estimate of errors
RMSE	root-mean-square error
CC	correlation coefficient
AM	additive manufacturing
FDM	fused deposition modeling
CAD	computer-aided design

REFERENCES

[1] Heuss, R, Müller, N., Sintern, W., Starke, A., and Tschiesner, A., 2012, *Lightweight, heavy impact: How carbon fiber and other lightweight materials will develop across industries and specifically in automotive*, Mckinsey & Company, editor.

[2] Strong, A. B., 2008, *Fundamentals of composites manufacturing: materials, methods and applications*. Society of Manufacturing Engineers.

[3] Koustoumpardis, P. N., and Aspragathos, N. A., 2004, "A review of gripping devices for fabric handling." *2014 23rd International Conference on Robotics in Alpe-Adria-Danube Region (RAAD)*, Smolenice, Slovakia, September 3-5, 2014, pp. 1-8.

[4] Trivedi, D., Rahn, C. D., Kier, W. M., and Walker, I. D, 2008, "Soft robotics: Biological inspiration, state of the art, and future research." *Applied bionics and biomechanics*, 5(3), pp. 99-117.

[5] Elder, H. M., and El-Tawashi, M., 1977, "Some bending measurements on yarns." *Journal of the Textile Institute*, 68, pp. 188-189.

[6] Taylor, P. M., 1995, "Presentation and gripping of flexible materials." *Assembly Automation*, 15(3), pp. 33-35.

[7] Seesselberg, H. A., 1990, "A challenge to develop fully automated garment manufacturing." *Sensory robotics for the handling of limp materials*, Berlin, Heidelberg, pp. 53-67

[8] Taylor, P. M., Pollett, D. M., and Grieβer, M. T., 1996, "Pinching grippers for the secure handling of fabric panels." *Assembly Automation*, 16(3), pp. 16-21.

[9] Ono, E., Ichijo, H., and Aisaka, N., 1992, "Flexible robotic hand for handling fabric pieces in garment manufacture." *International Journal of Clothing Science and Technology*, 4(5), pp. 16-23.

[10] Ono, E., Okabe, H., Akami, H., and Aisaka, N., 1991, "Robot hand with a sensor for cloth handling." *Journal of the textile machinery society of Japan*, 37(1), pp. 14-24.

[11] Kolluru, R., Valavanis, K. P., Steward, A., and Sonnier, M. J., 1995, "A flat surface robotic gripper for handling limp material." *IEEE Robotics & Automation Magazine*, 2(3), pp. 19-26.

[12] Hebert, T. M., Valavanis, K. P., and Kolluru, R., 1997, April, "A robotic gripper system for limp material manipulation: Hardware and software development and integration." *Proceedings of International Conference on Robotics and Automation*, Albuquerque, NM, USA, vol. 1, pp. 15-21.

[13] Kolluru, R., Valavanis, K. P., and Hebert, T. M., 1998, "Modeling, analysis, and performance evaluation of a robotic gripper system for limp material handling." *IEEE Transactions on Systems, Man, and* Cybernetics, Part B (Cybernetics), 28(3), pp. 480-486.

[14] Fleischer, J., Ochs, A., and Förster, F., 2013, "Gripping Technology for Carbon Fibre Material." *CIRP International conference on competitive manufacturing*, pp. 65-71.

[15] Fleischer, J., Förster, F. and Crispieri, N., 2014, "Intelligent gripper technology for the handling of carbon fiber material." *Production Engineering*, *8*(6), pp. 691-700.

[16] Sun, B., and Zhang, X., 2019, "A New Electrostatic Gripper for Flexible Handling of Fabrics in Automated Garment Manufacturing." *2019 IEEE 15th International Conference on Automation Science and Engineering (CASE)*, Vancouver, BC, Canada, pp. 879-884.

[17] Costo, S., G. Altamura, L. E. Bruzzone, R. M. Molfino, and Zoppi, M., 2002, "Design of a re-configurable gripper for the fast robotic picking and handling of limp sheets." *Proceedings of the 33rd International Symposium on Robotics*, Stockholm, Sweden, October 7-11, 2002.

[18] Kordi, M., Tarsha, M. Husing, and Corves, B., 2007, "Development of a multifunctional robot end-effector system for automated manufacture of textile preforms." *2007 IEEE/ASME international conference on advanced intelligent mechatronics*, Zurich, Switzerland, 4-7 September 2007, pp. 1-6.

[19] Ragunathan, S., and L. Karunamoorthy, 2008, "Modular reconfigurable robotic gripper for limp material handling in garment industries." *International journal of robotics & automation*, 23(4), pp. 213.

[20] Flixeder, S., Tobias G., and Kug, A., 2017, "Force-based cooperative handling and lay-up of deformable materials: Mechatronic design, modeling, and control of a demonstrator." *Mechatronics*, 47, pp. 246-261.

[21] Doulgeri, Z., and Fahantidis, N., 2002, "Picking up flexible pieces out of a bundle." *IEEE robotics & automation magazine*, 9(2), pp. 919.

[22] Murakami, K., and Hasegawa, T., 2004, "Novel fingertip equipped with soft skin and hard nail for dexterous multi-fingered robotic manipulation." *Journal of the Robotics Society of Japan*, 22(5), pp. 616-624.

[23] Koustoumpardis, P., Nastos, K., and Aspragathos, N., 2014, "Underactuated 3-finger robotic gripper for grasping fabrics." *2014 23rd International Conference on Robotics in Alpe-Adria-Danube Region (RAAD)*, Smolenice, Slovakia, September 3-5, 2014, pp. 1-8.

[24] Alebooyeh, M., Wang, B., Urbanic, R. J., Djuric, A., and Kalami, H., 2019, "Investigating Collaborative Robot Gripper Configurations for Simple Fabric Pick and Place Tasks." *SAE Technical Paper*, DOI: 10.4271/2019-01-0699.

[25] Alebooyeh, M., Wang, B., and Urbanic, R. J., 2020, "Performance Study of an Innovative Collaborative Robot Gripper Design on Different Fabric Pick and Place Scenarios." *SAE Technical Paper*, DOI: 10.4271/2020-01-1304.

[26] Birglen, L., Gosselin, C., and Laliberté, T., 2008, *Underactuated robotic hands*. Springer.

[27] Kim, S., Laschi, C., and Trimmer, B., 2013, "Soft robotics: a bioinspired evolution in robotics." *Trends in biotechnology*, 31(5), pp. 287-294.

[28] Shintake, J., Cacucciolo, V., Floreano, D., and Shea, H., 2018, "Soft robotic grippers." Advanced Materials, 30(29), 1707035.

[29] Ilievski, F., Mazzeo, A. D., Shepherd, R. F., Chen, X., and Whitesides, G. M., 2011, "Soft robotics for chemists." *Angewandte Chemie International Edition*, 50(8), pp. 1890-1895.

[30] Hao, Y., Wang, T., Ren, Z., Gong, Z., Wang, H., Yang, X., ... and Wen, L., 2017, "Modeling and experiments of a soft robotic gripper in amphibious

environments." *International Journal of Advanced Robotic Systems*, 14(3), 1729881417707148.

[31] Mooney, M., 1940, "A theory of large elastic deformation." *Journal of applied physics*, *11*(9), pp. 582-592.

[32] Rivlin, R. S., 1948, "Large elastic deformations of isotropic materials IV. Further developments of the general theory." *Philosophical Transactions of the Royal Society of London. Series A, Mathematical and Physical Sciences*, *241*(835), pp. 379-397.

[33] Ogden, R. W., 1984, *Non-linear elastic deformations*. Courier Corporation, NY, USA.

[34] Martins, P. A. L. S., Natal Jorge, R. M., and Ferreira, A. J. M., 2006, "A comparative study of several material models for prediction of hyperelastic properties: Application to silicone-rubber and soft tissues." *Strain*, *42*(3), pp. 135-147.

[35] Korochkina, T. V., Jewell, E. H., Claypole, T. C., and Gethin, D. T., 2008, "Experimental and numerical investigation into nonlinear deformation of silicone rubber pads during ink transfer process." *Polymer Testing*, 27(6), pp. 778-791.

[36] Rachik, M., Schmidtt, F., Reuge, N., Le Maoult, Y., and Abbeé, F., 2001, "Elastomer biaxial characterization using bubble inflation technique. II: Numerical investigation of some constitutive models." *Polymer Engineering & Science*, 41(3), pp. 532-541.

[37] Gent, A. N., 2012, *Engineering with rubber: how to design rubber components*. Carl Hanser Verlag GmbH Co KG.

[38] Jauffrès, D., Sherwood, J. A., Morris, C. D., and Chen, J., 2010, "Discrete mesoscopic modeling for the simulation of woven-fabric reinforcement forming." *International journal of material forming*, 3(2), pp. 1205-1216.

[39] Nasri, M., Garnier, C., Abbassi, F., Labanieh, A. R., Dalverny, O., and Zghal, A., 2019, "Hybrid approach for woven fabric modelling based on discrete hypoelastic behaviour and experimental validation." *Composite Structures*, 209, pp. 992-1004.

[40] Diehl, T., Dixon, R. D., Lamontia, M. A., and Hanks, J. A., 2003, "The development and use of a robust modeling approach for predicting structural performance of woven fabric using ABAQUS." *2003 ABAQUS Users' Conference*.

[41] Eischen, J. W., Deng, S., and Clapp, T. G., 1996, "Finite-element modeling and control of flexible fabric parts." *IEEE Computer Graphics and Applications*, 16(5), pp. 71-80.

Figure Captions List

a. Picking up a single ply; b. Separating a ply from a stack; c. De-wrinkling

Fig. 35 Comparison between experimental data and simulation data

Table Caption List

Figure List

Fig. 1

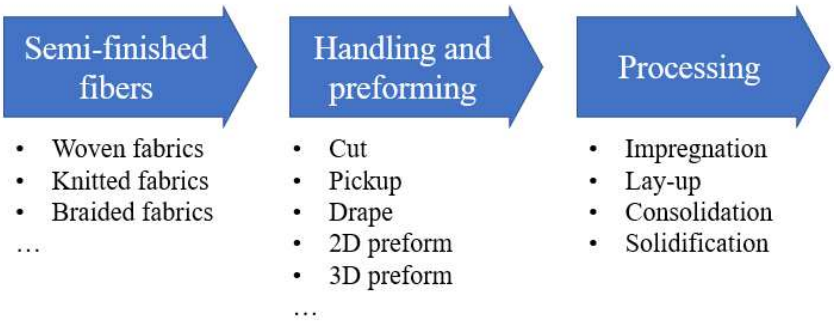

Fig. 2

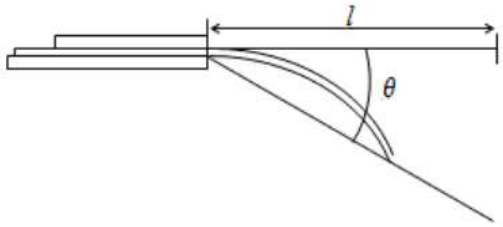

Fig. 3

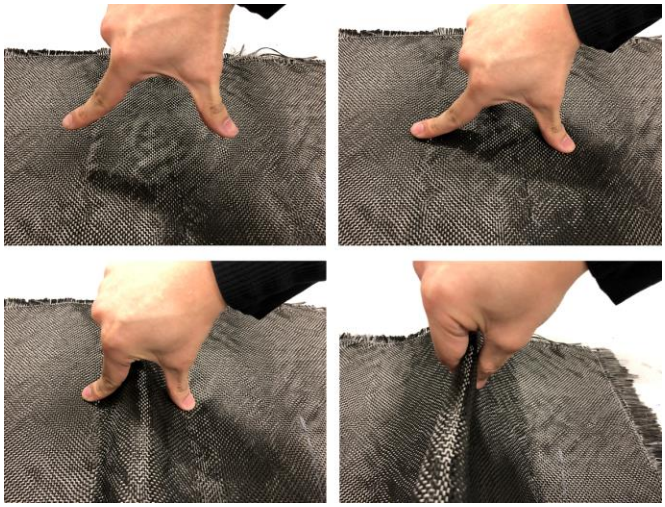

Fig. 4

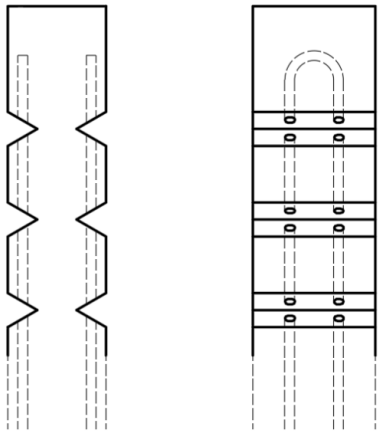

Fig. 5

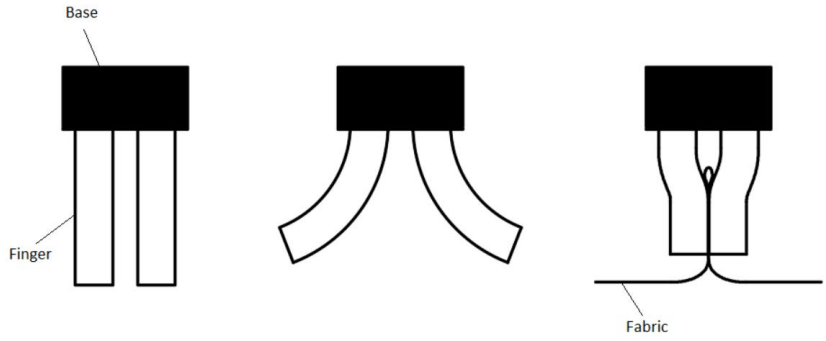

Fig. 6

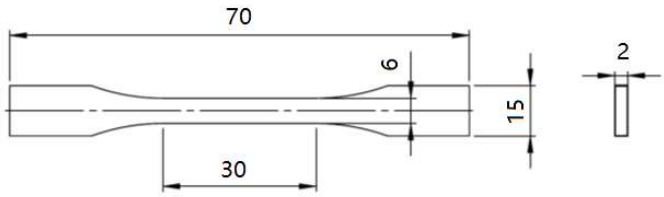

Fig. 7

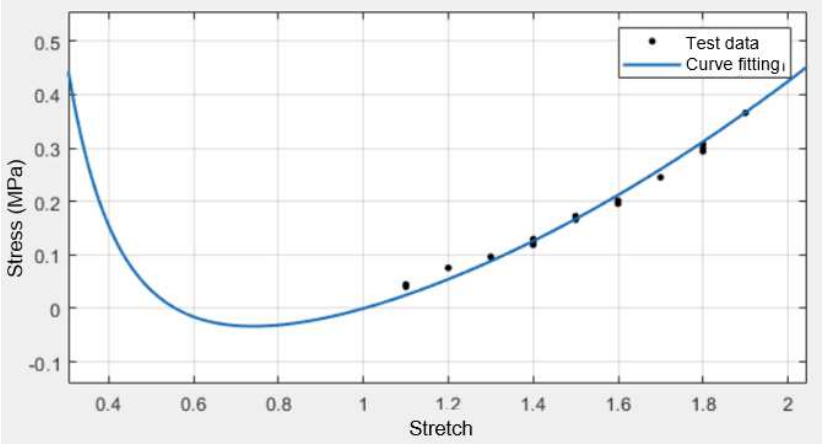
Test data
Curve fitting
Stress (MPa)
Stretch
0.5
0.4
0.3
0.2
0.1
0
-0.1
0.4
0.6
0.8
1
1.2
1.4
1.6
1.8
2

Fig. 8

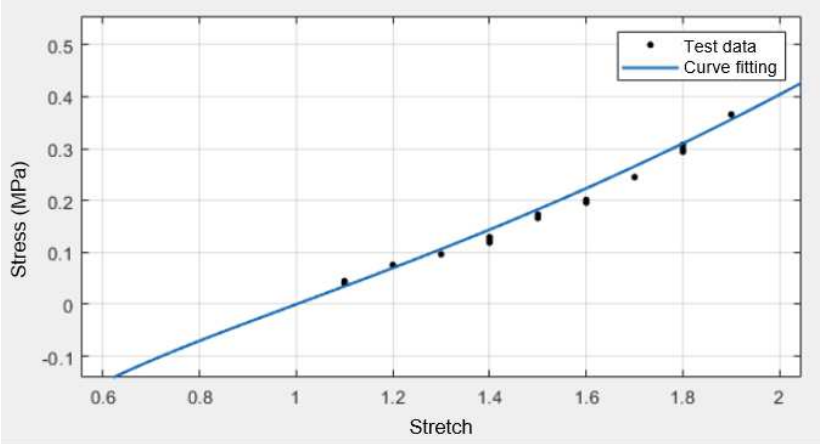
Test data
Curve fitting
Stress (MPa)
Stretch
0.5
0.4
0.3
0.2
0.1
0
-0.1
0.6
0.8
1
1.2
1.4
1.6
1.8
2

Fig. 9

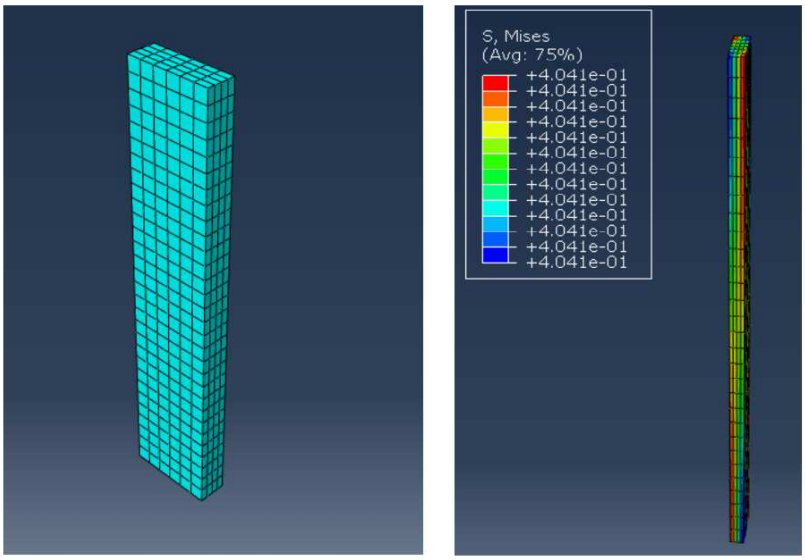
S, Mises
(Avg: 75%)
+4.041e-01
+4.041e-01
+4.041e-01
+4.041e-01
+4.041e-01
+4.041e-01
+4.041e-01
+4.041e-01
+4.041e-01
+4.041e-01
+4.041e-01
+4.041e-01

a b

Fig. 10

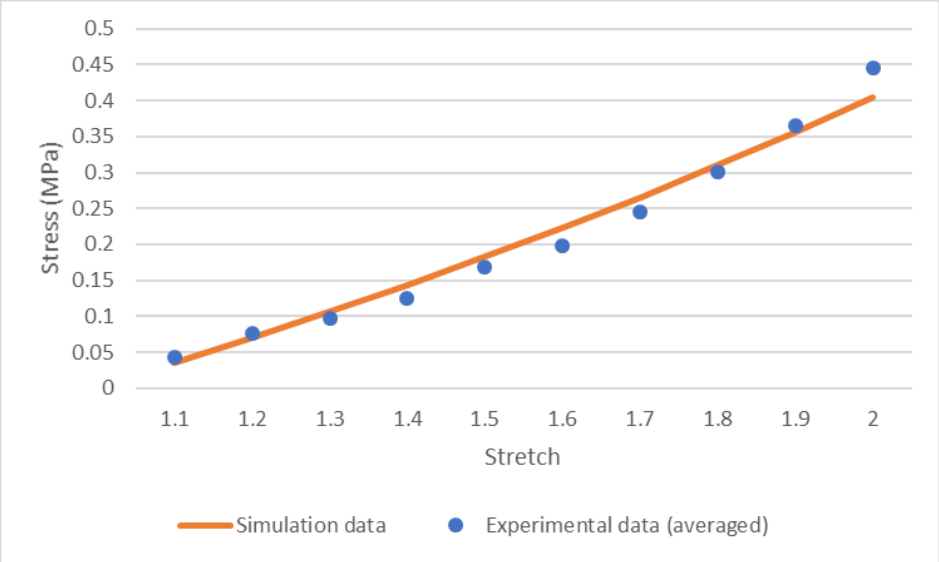
0.5
0.45
0.4
0.35
0.3
0.25
0.2
0.15
0.1
0.05
0
Stress (MPa)
1.1
1.2
1.3
1.4
1.5
1.6
1.7
1.8
1.9
2
Stretch
Simulation data
Experimental data (averaged)

Fig. 11

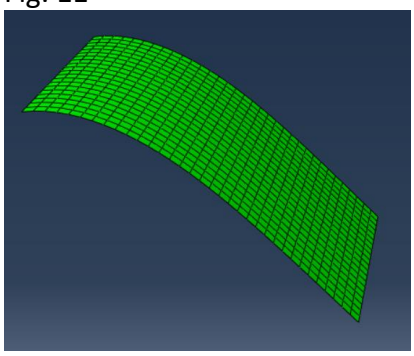

Fig. 12

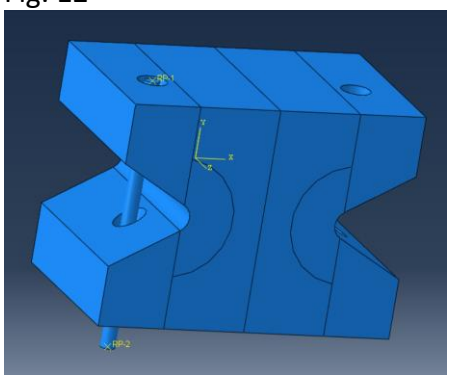

Fig. 13

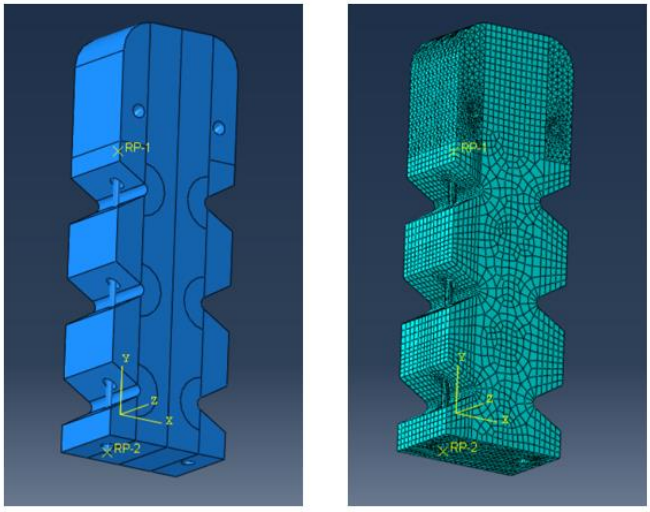

a b

Fig. 14

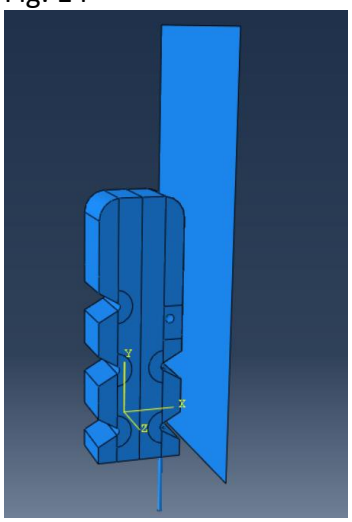

Fig. 15

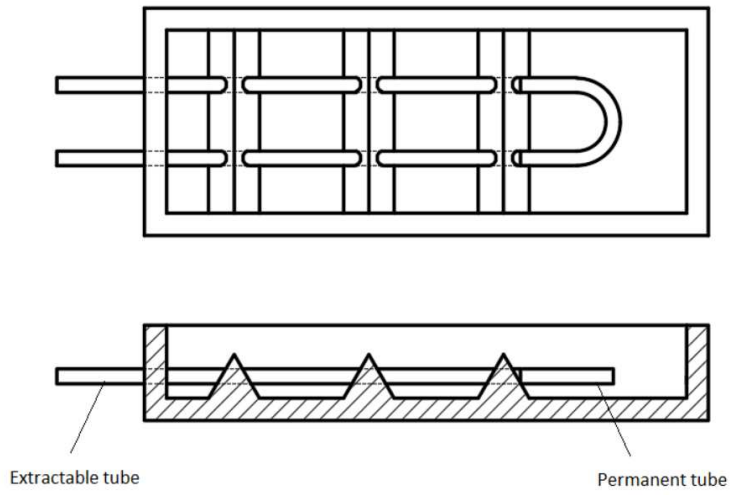

Fig. 16

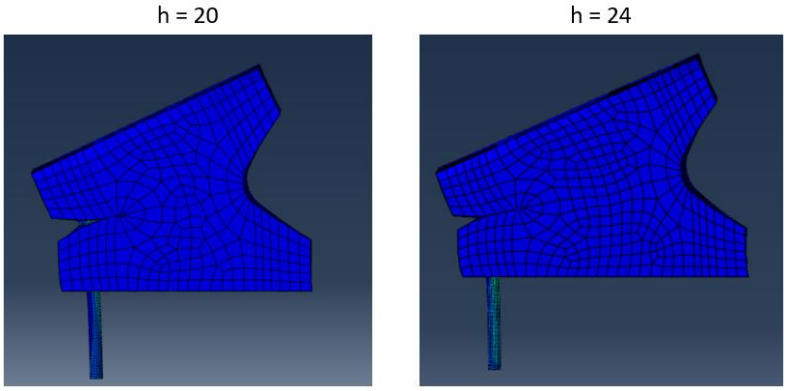

Fig. 17

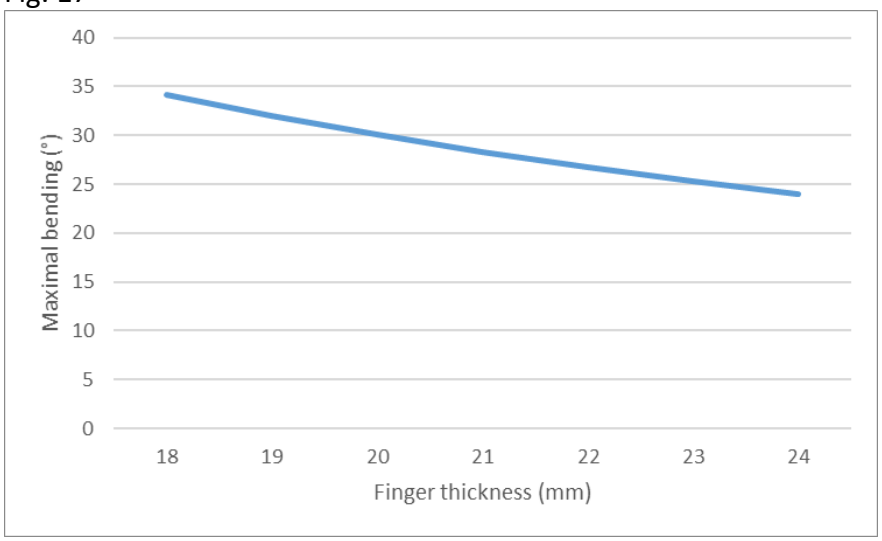
40
35
30
25
20
15
10
5
0
Maximal bending (°)
18
19
20
21
22
23
24
Finger thickness (mm)

Fig. 18

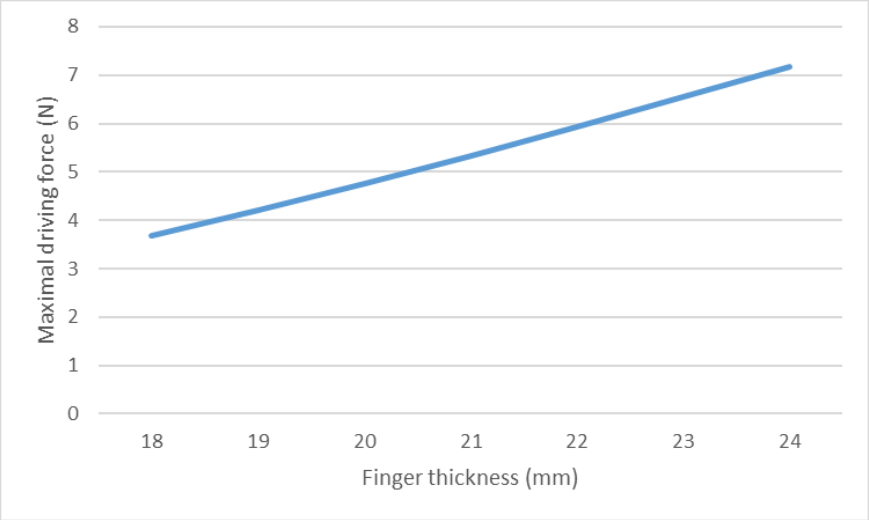
8
7
6
5
4
3
2
1
0
Maximal driving force (N)
18
19
20
21
22
23
24
Finger thickness (mm)

Fig. 19

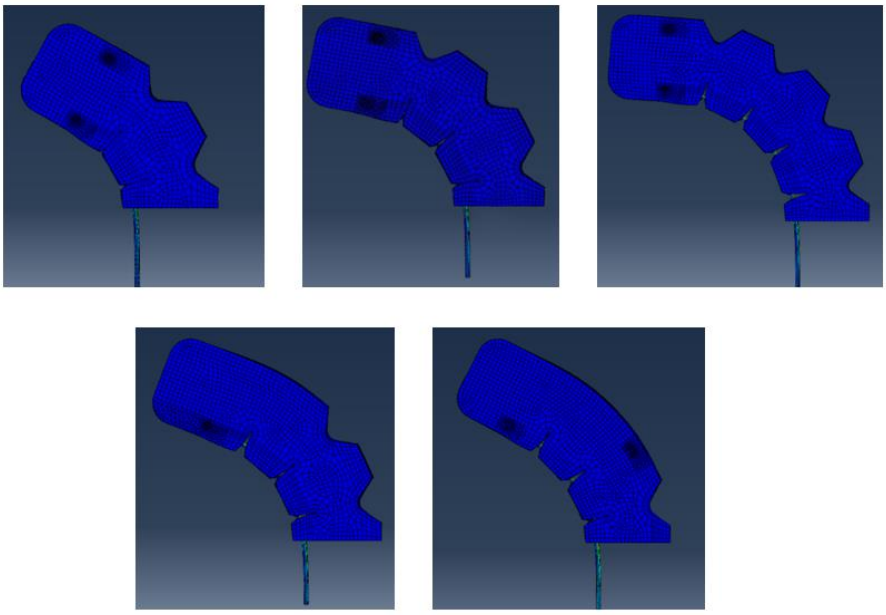

Fig. 20

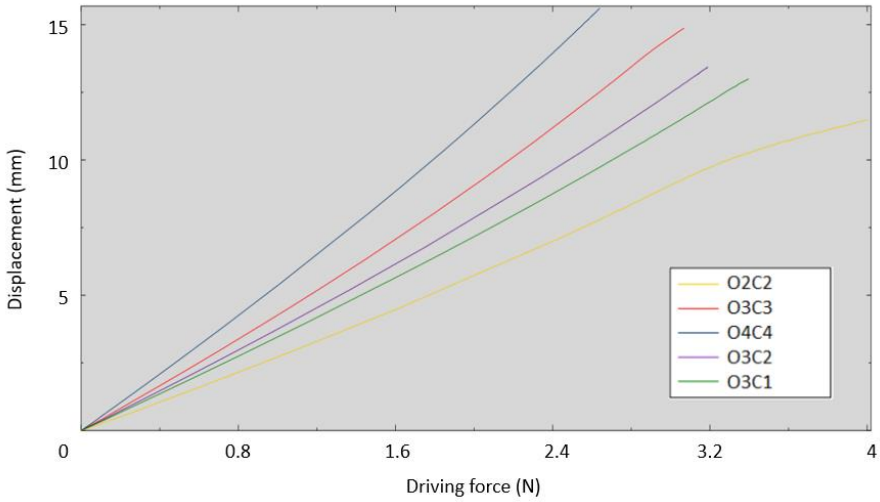
15
10
5
0
0.8
1.6
2.4
3.2
4
Displacement (mm)
Driving force (N)
O2C2
O3C3
O4C4
O3C2
O3C1

Fig. 21

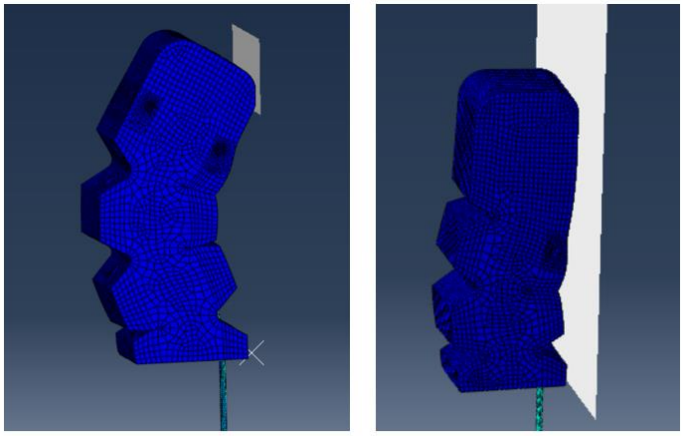

a b

Fig. 22

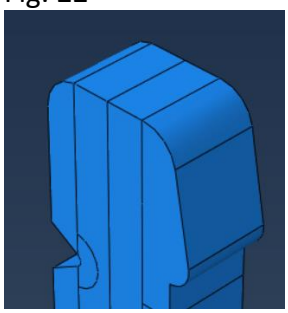

Fig. 23

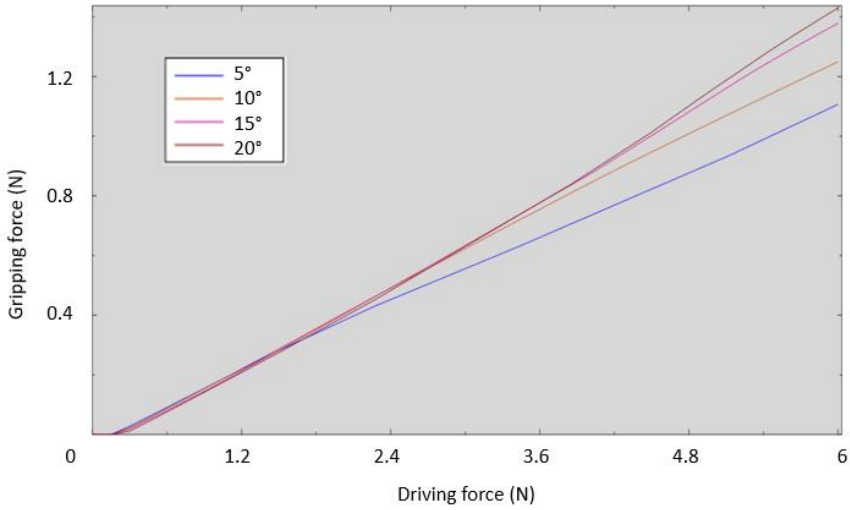
5°
10°
15°
20°
Gripping force (N)
1.2
0.8
0.4
0
1.2
2.4
3.6
4.8
6
Driving force (N)

Fig. 24

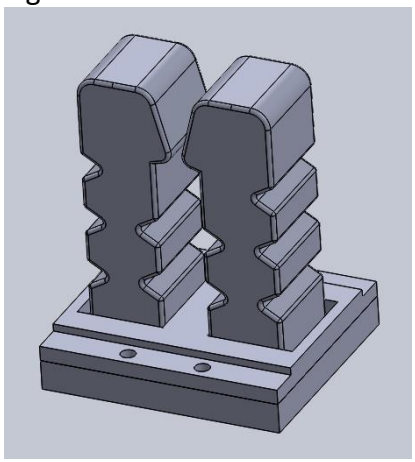

Fig. 25

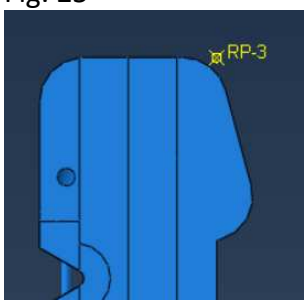

Fig. 26

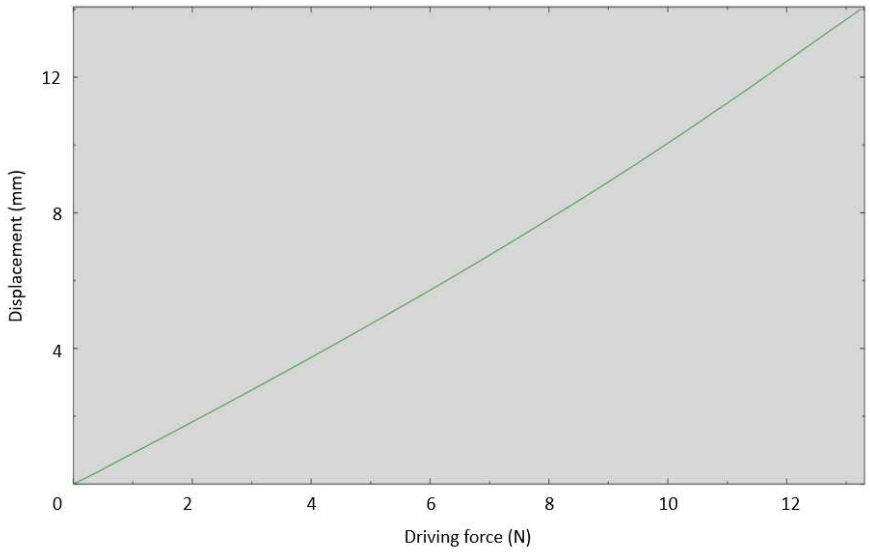

Fig. 27

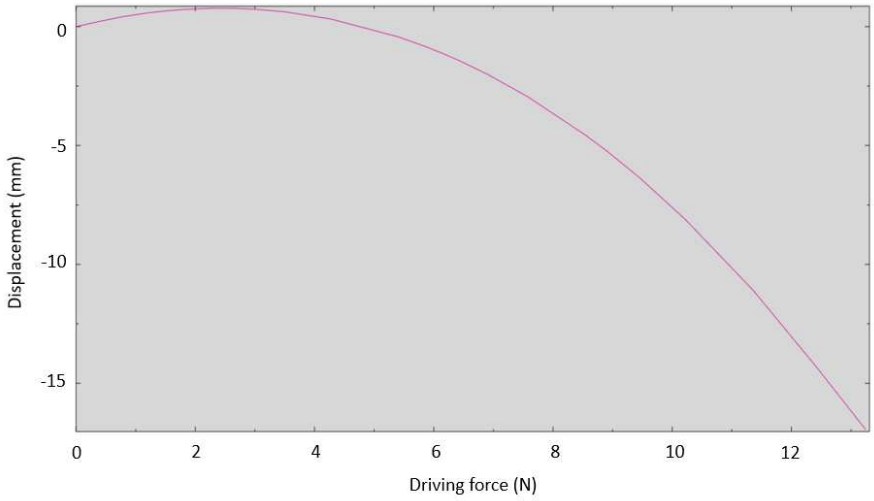

Fig. 28

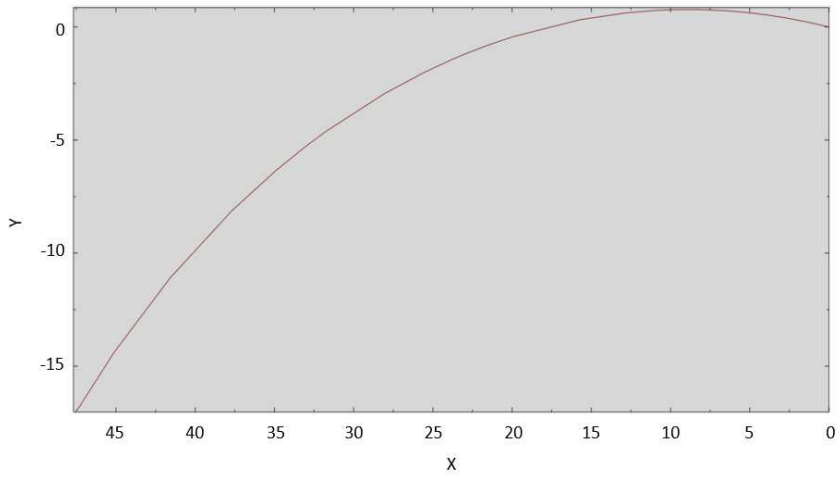

Fig. 29

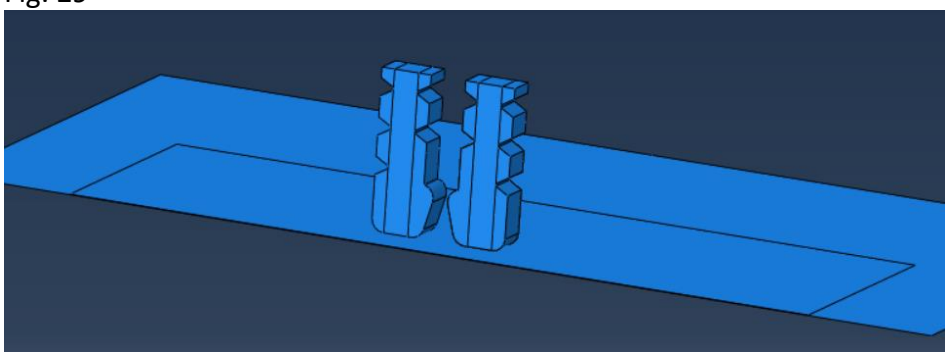

Fig. 30

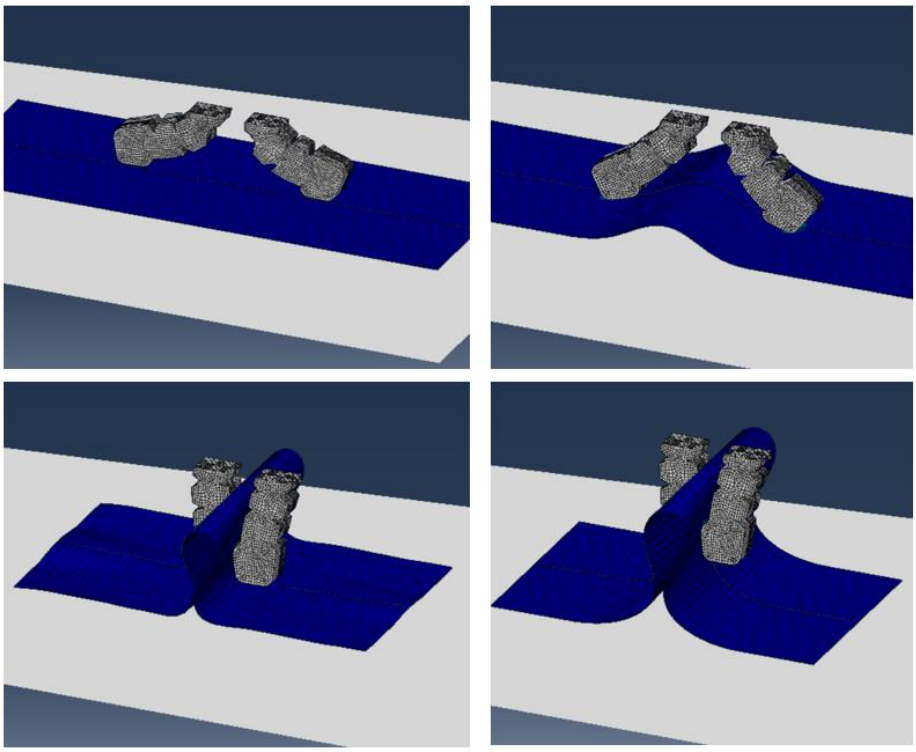

Fig. 31

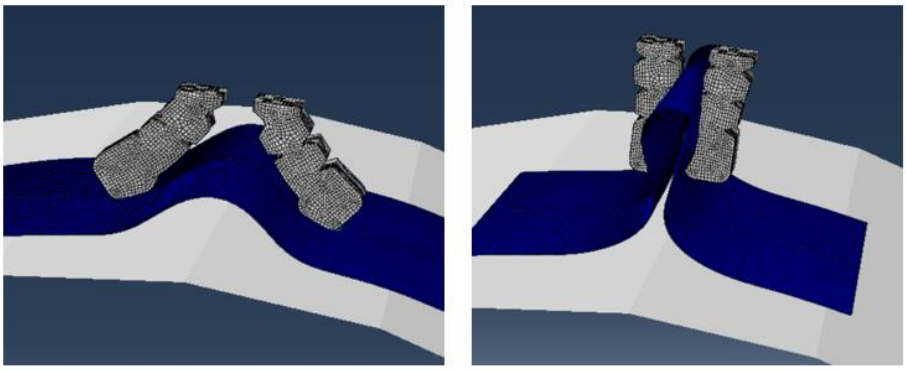

Fig. 32

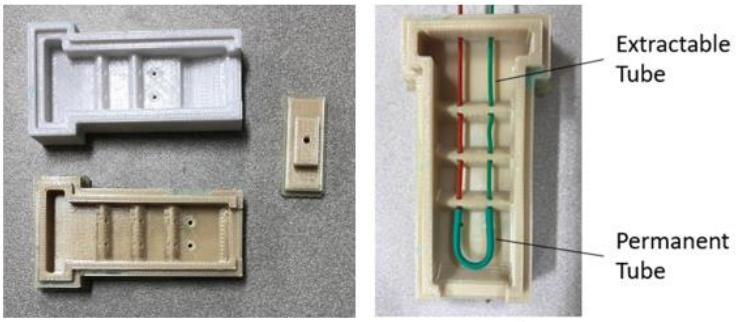

Fig. 33

Fig. 34

a) b) c)

Fig. 35

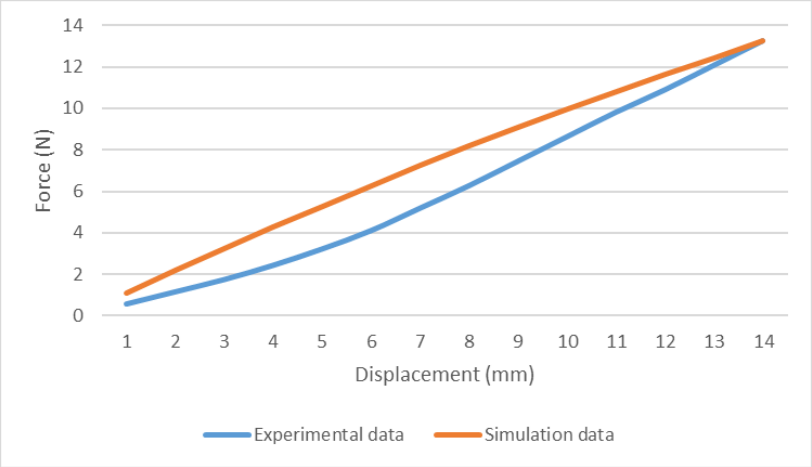
14
12
10
8
6
4
2
0
Force (N)
1
2
3
4
5
6
7
8
9
10
11
12
13
14
Displacement (mm)
Experimental data
Simulation data

Table List

Table 1

Style	Complexity	Actuation speed	Gripping force
Compliant structure	◔	●	◑
Tendon actuation	◑	●	◕
Pneumatic actuation	●	◕	●

Table 2

Reusable	Printing the mold set	2h35m
	Removing support material	3h
Molding silicone fingers		1h * 2
Printing the gripper base		1h26m
Removing support material		30m
Total		9h31m **/ 3h56m**

Table 3

Size (mm)	Normal	Max open
	93 * 55 * 47	66 *135 * 47
Weight (g)	Gripper	One finger
	127.5	41
Max open angle (°)	180	
Max open length (mm)	135	
Max bending radius (mm)	14.4	
Max contact area (mm^2)	375	

Figures

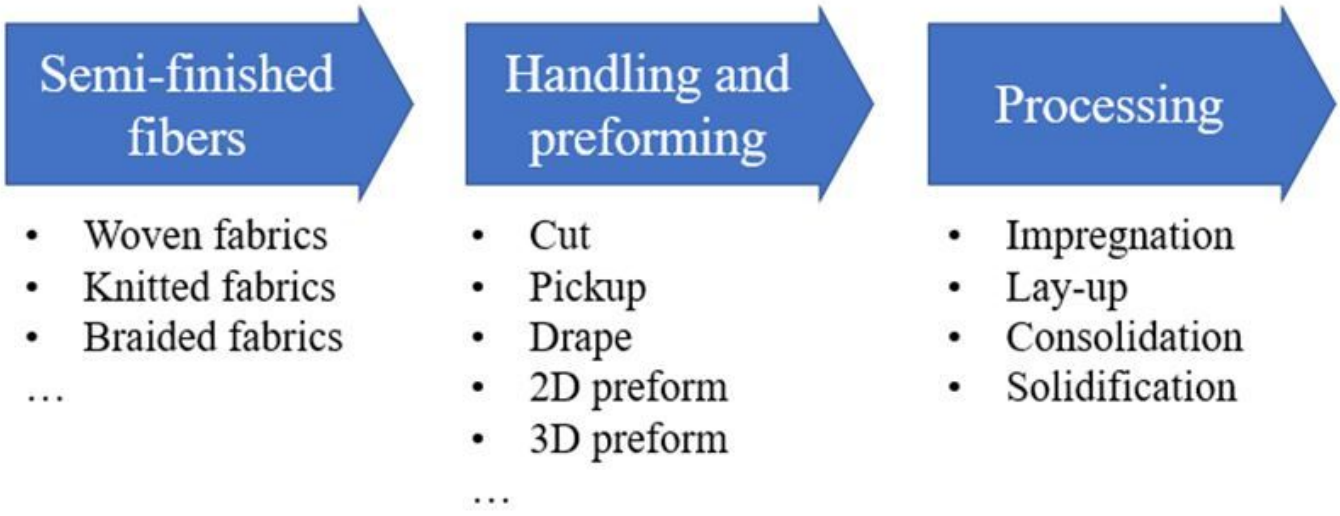

Figure 1

Stages of composites manufacturing

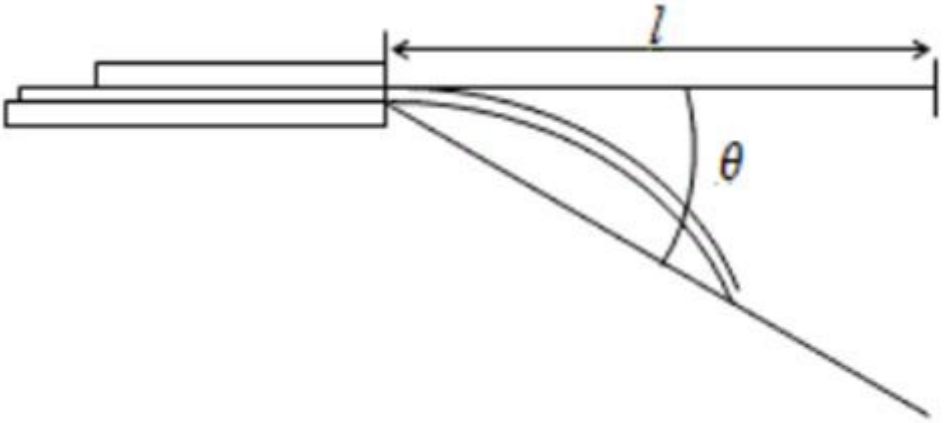

Figure 2

Peirce's cantilever method

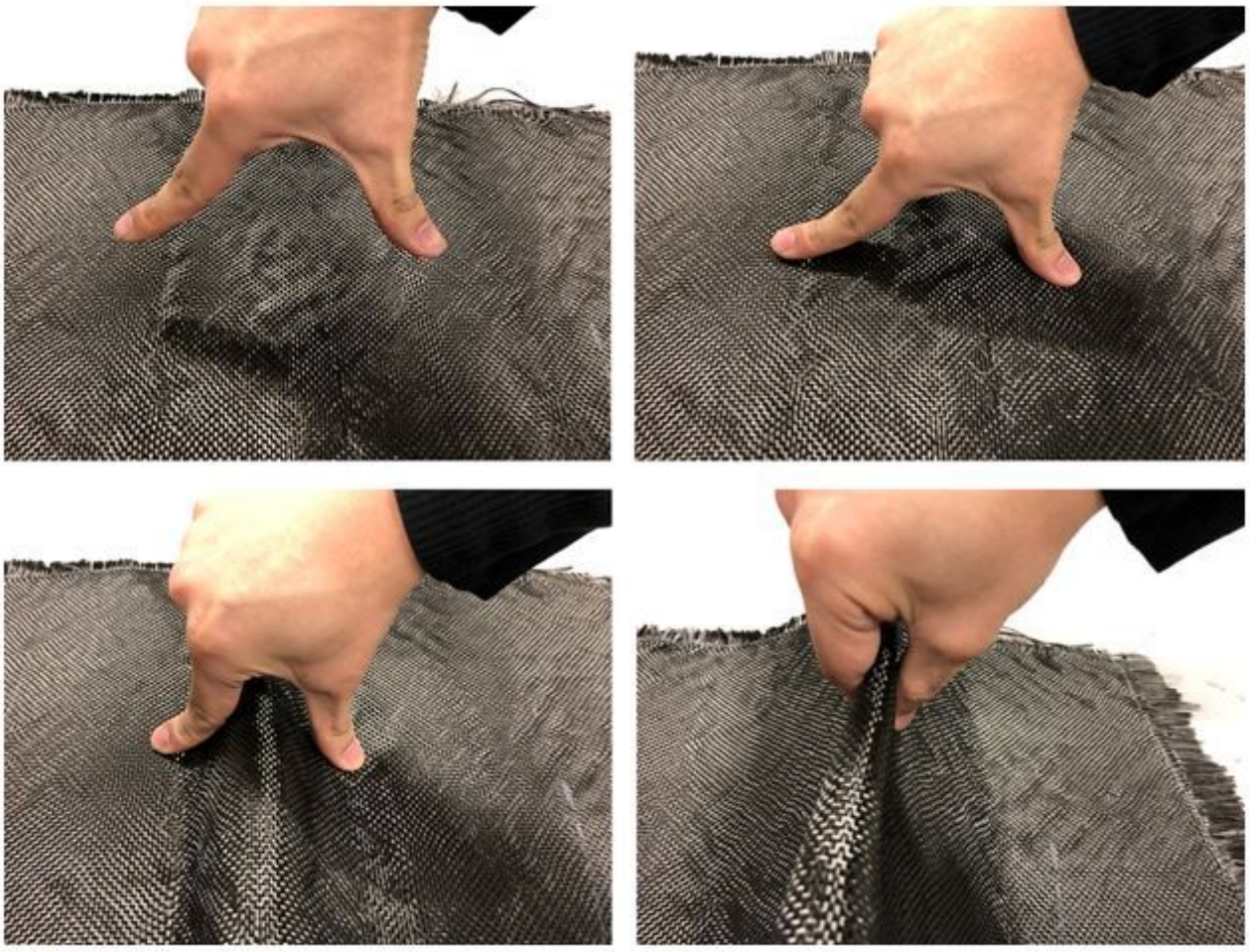

Figure 3

Manual picking

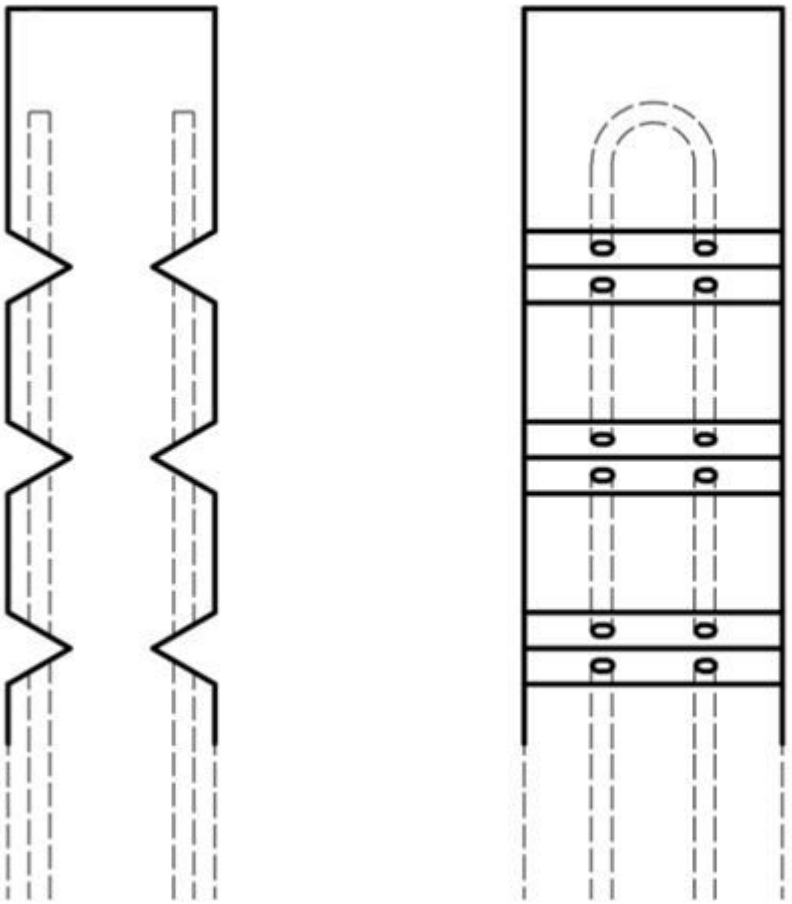

Figure 4

Cable actuated gripper configuration

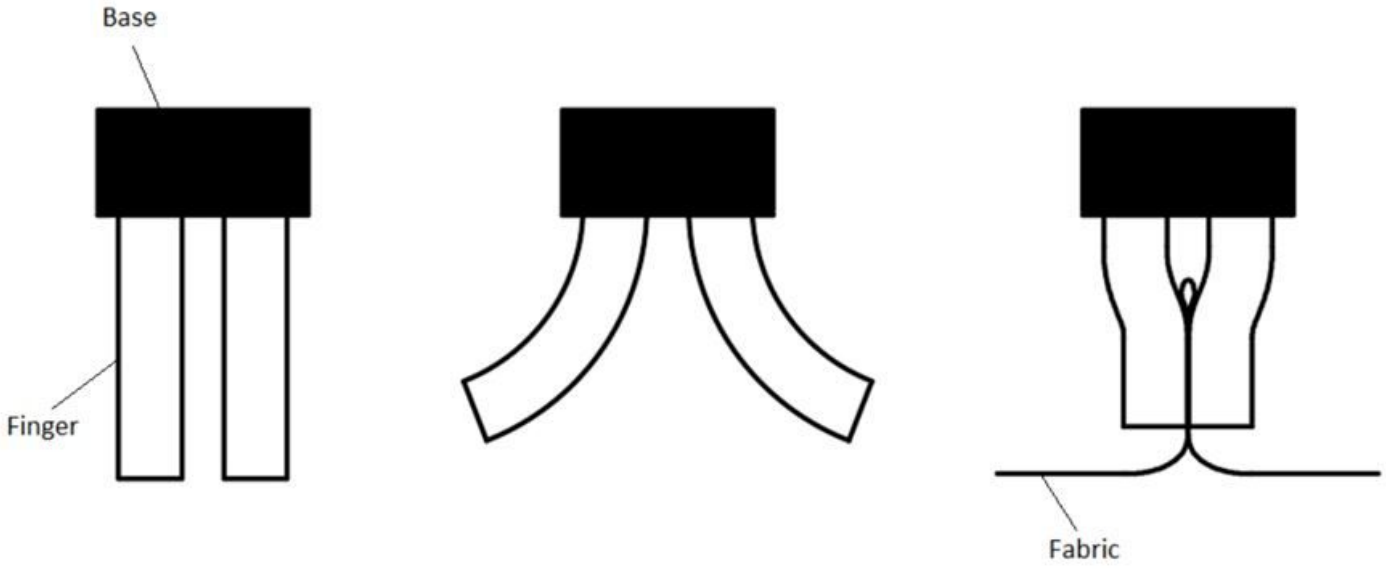

Figure 5

Postures of a conceptual gripper configuration

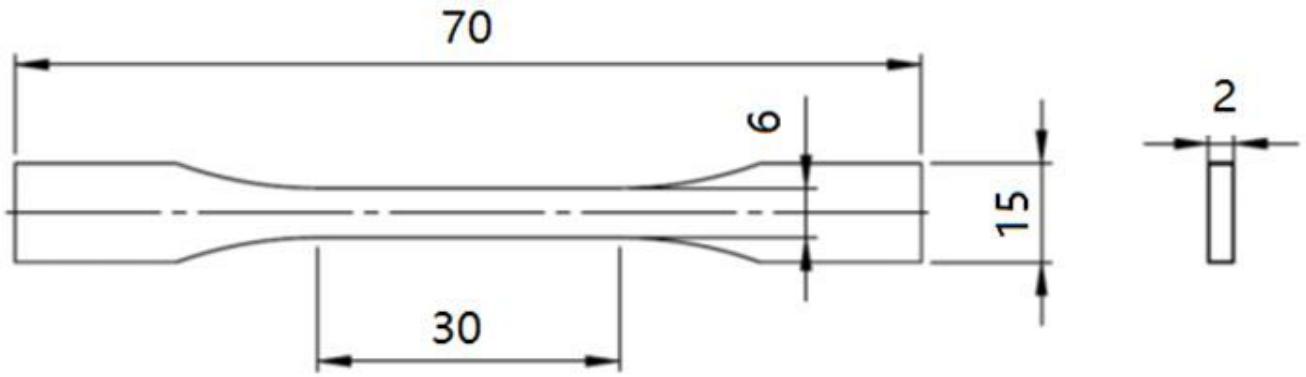

Figure 6

Dumbbell-shape sample

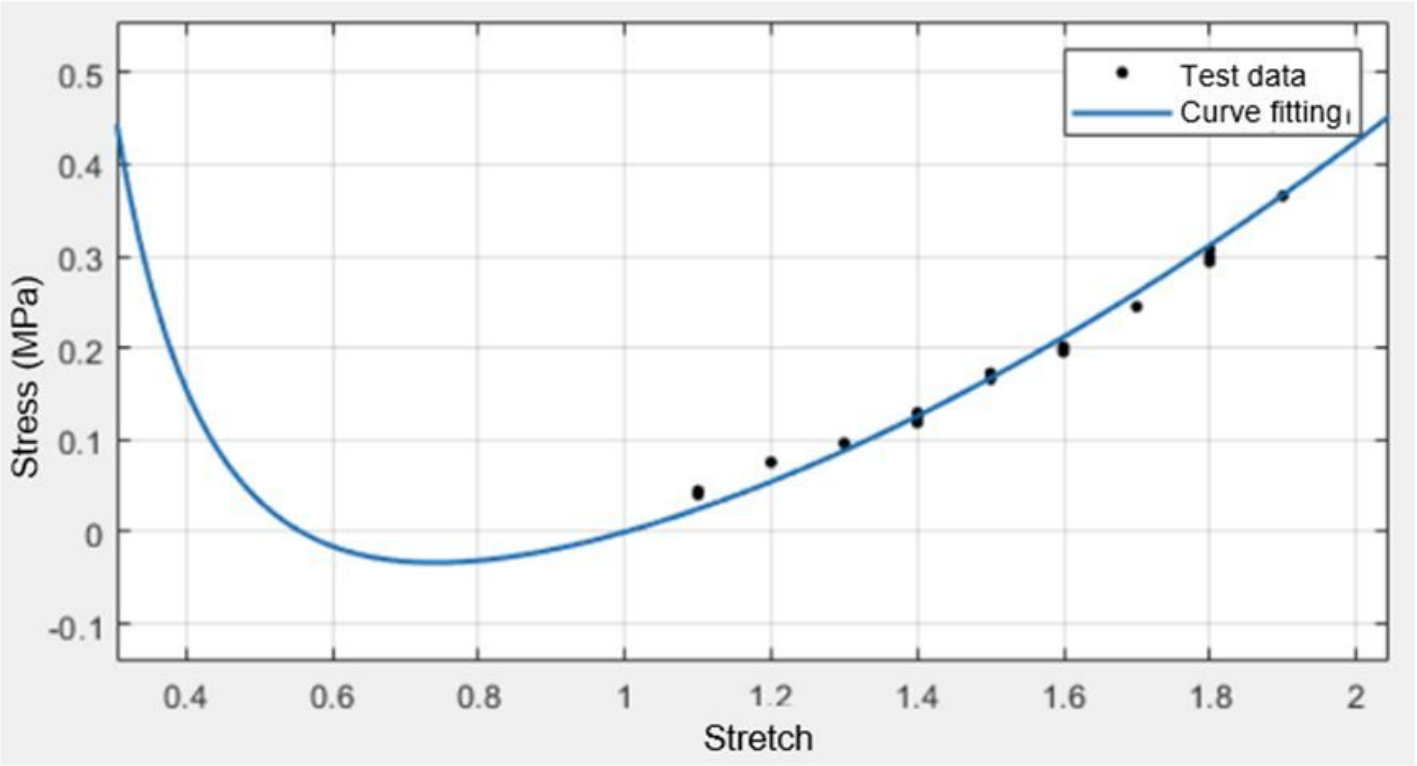

Figure 7

Fitting result

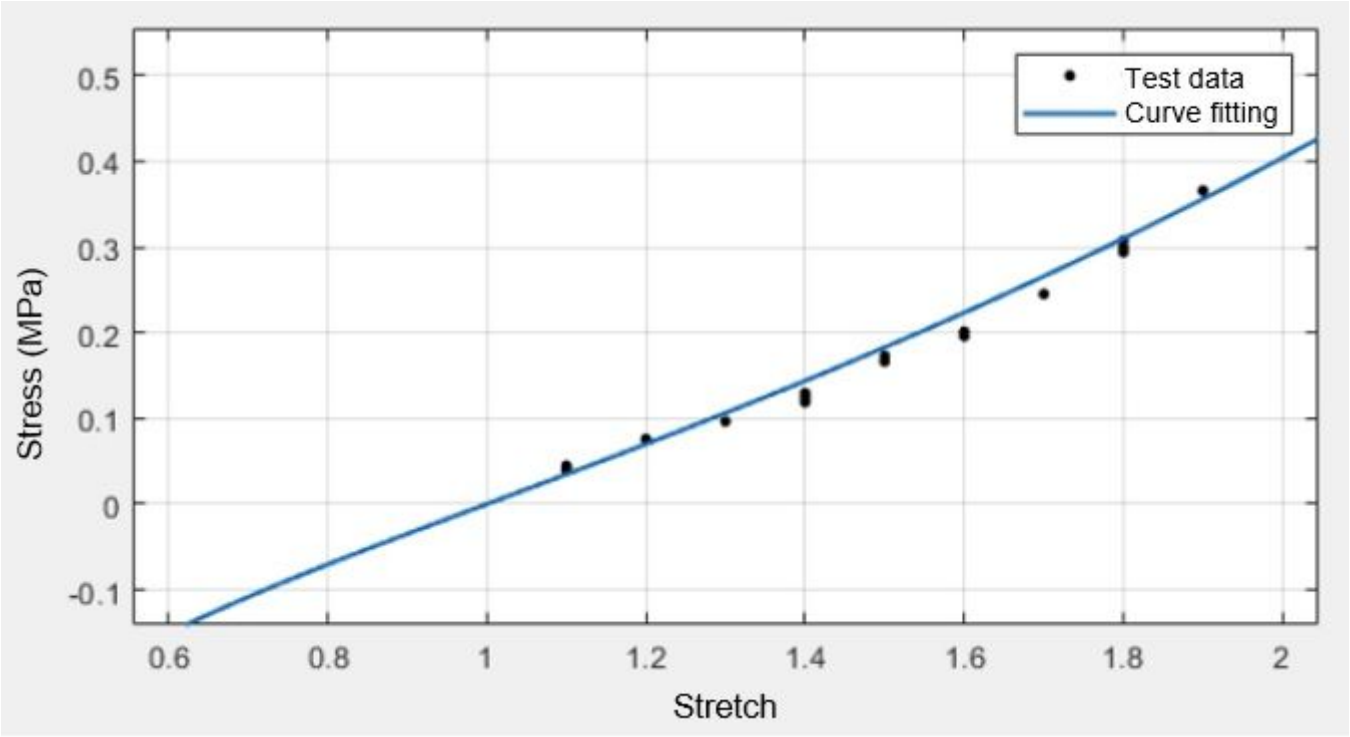

Figure 8

Modified fitting result

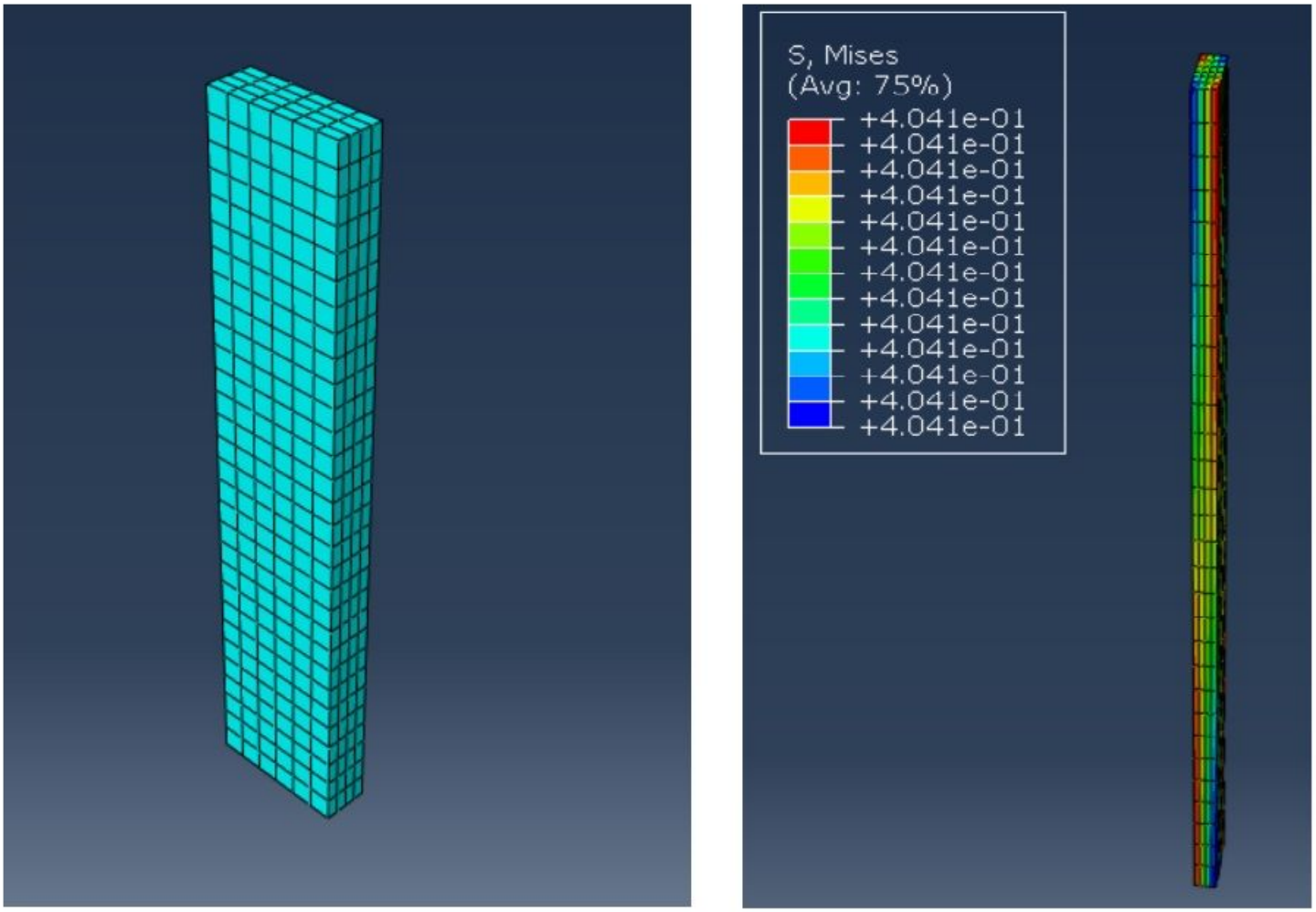

Figure 9

Modified fitting result a. Meshed model; b. Simulation result

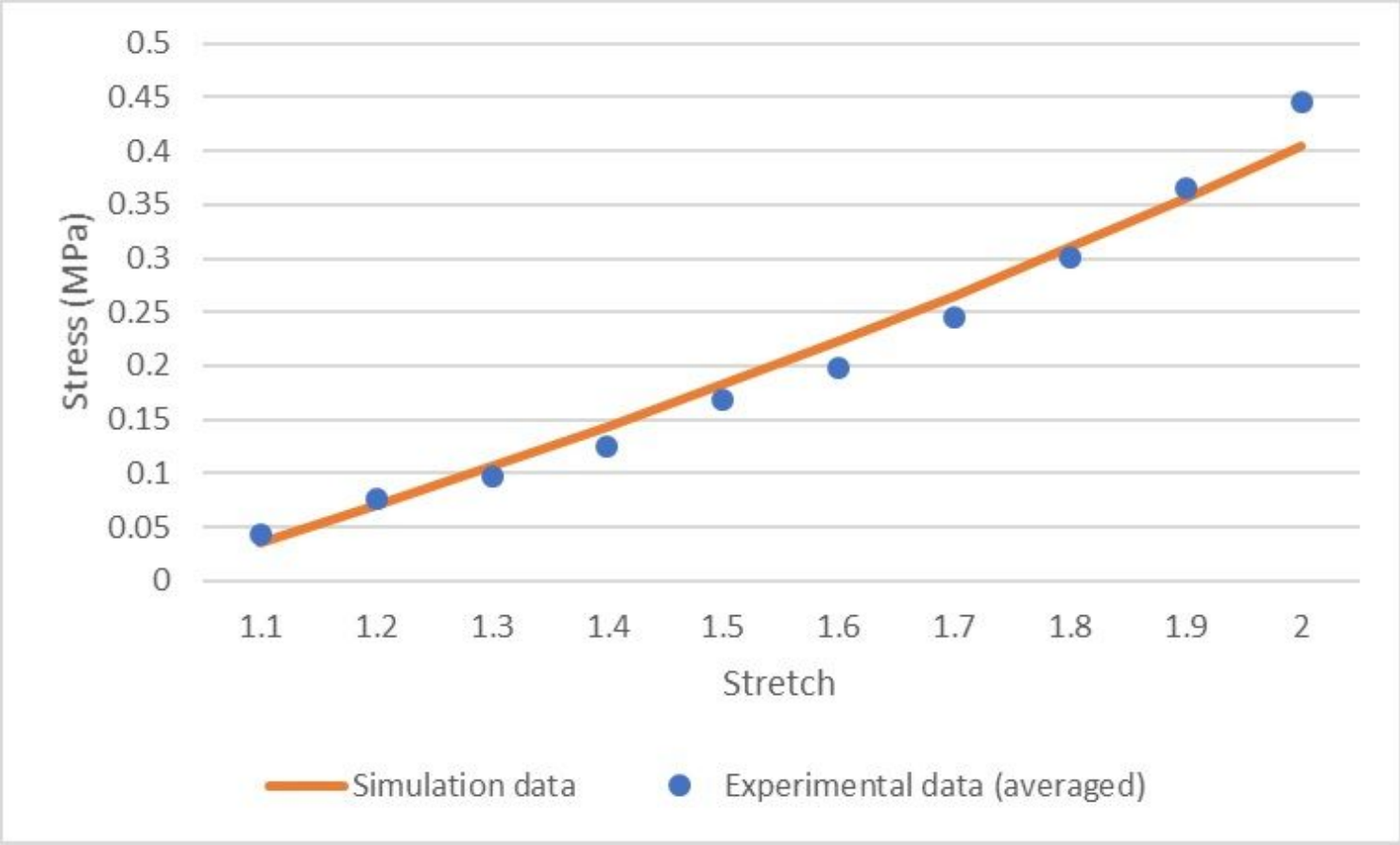

Figure 10

Comparison between FEA result and the test data

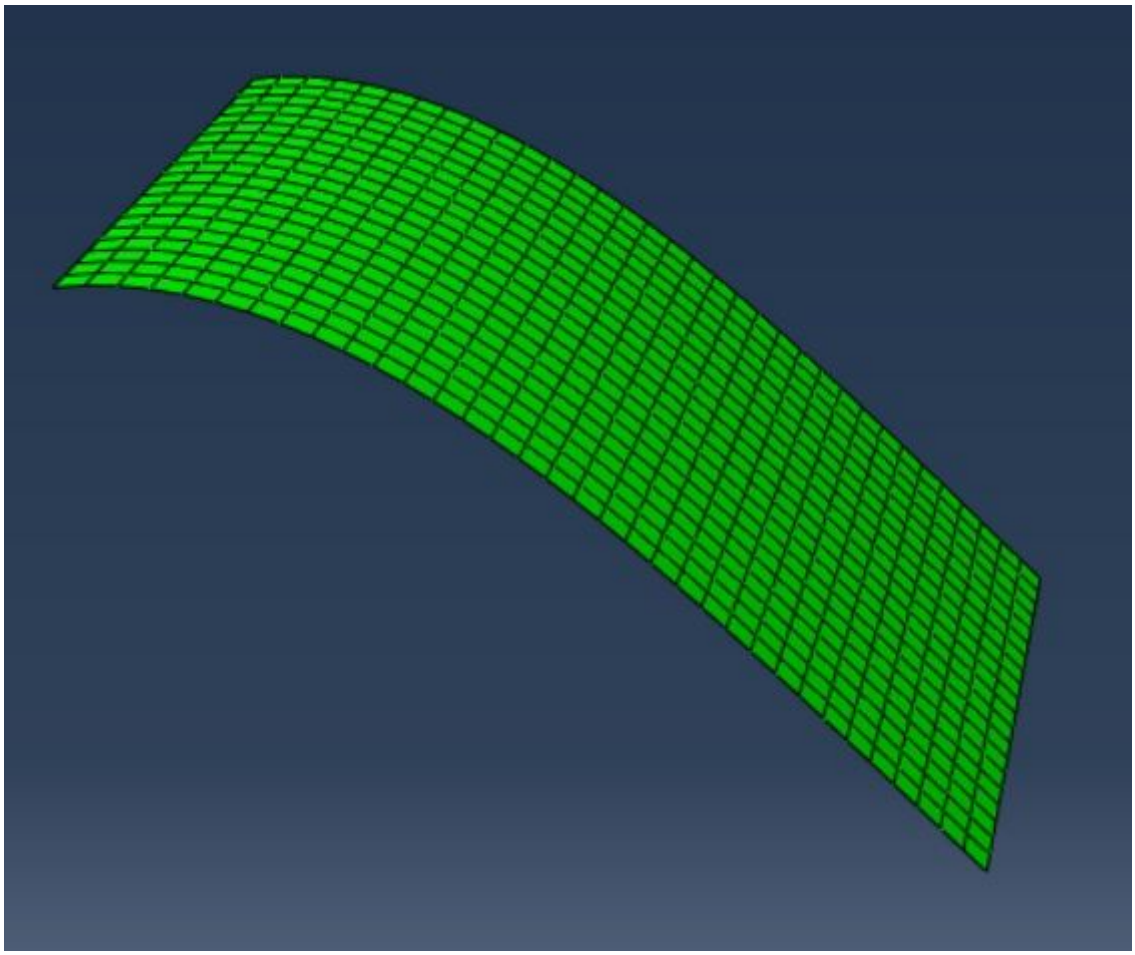

Figure 11

Draping result of the simplified fabric model

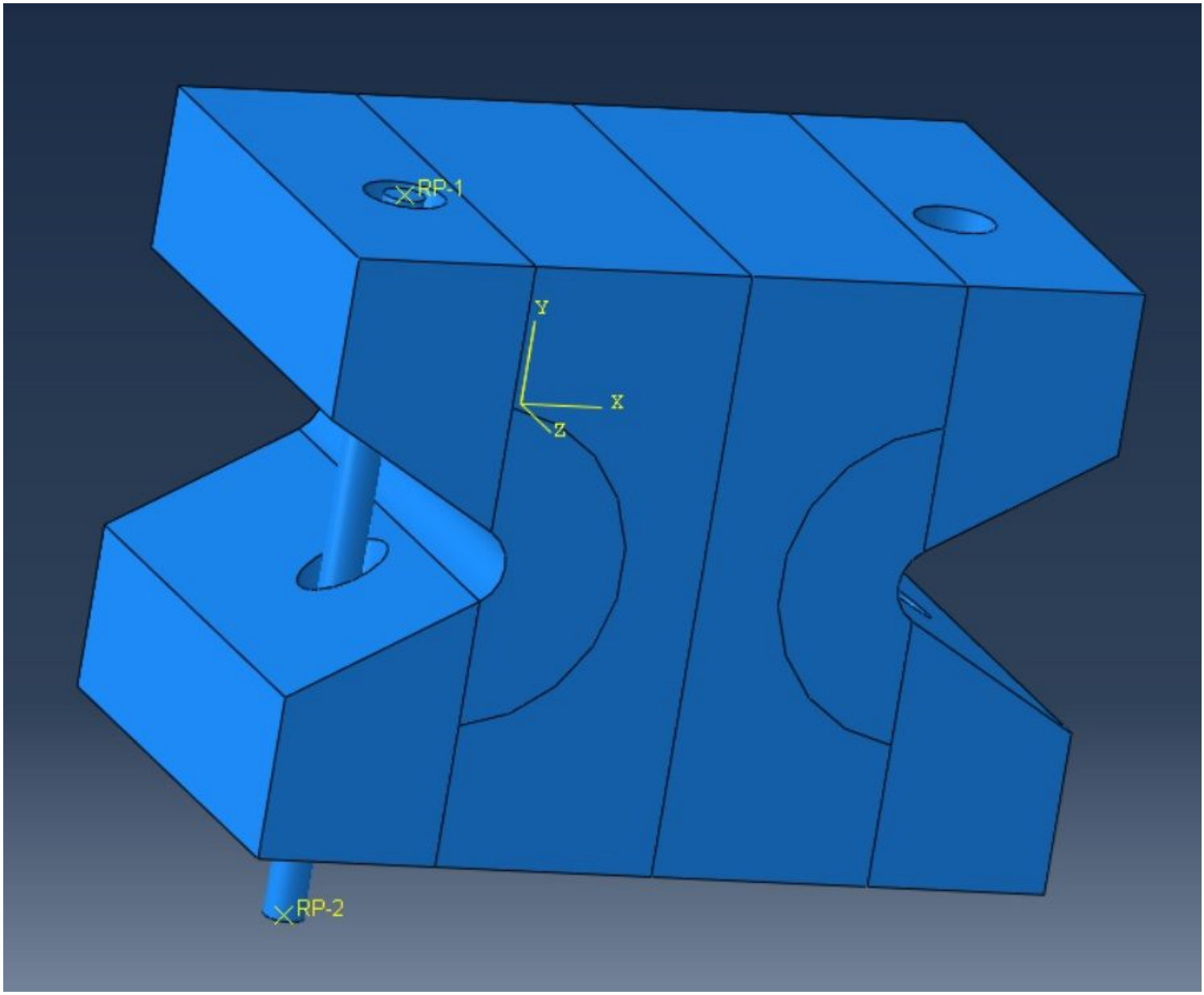

Figure 12

FE model of a unit section

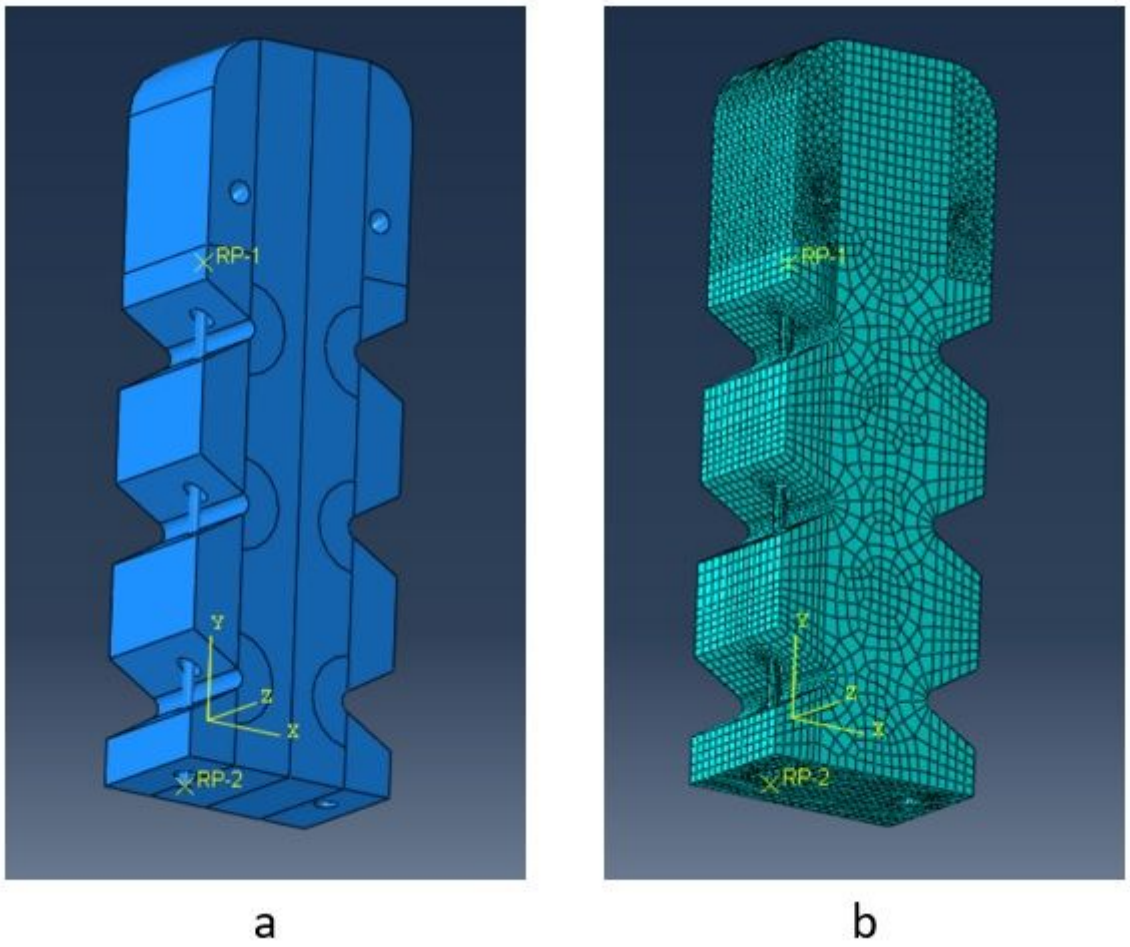

a b

Figure 13

FE model of the elastomer finger a. Assembly; b. Meshed model

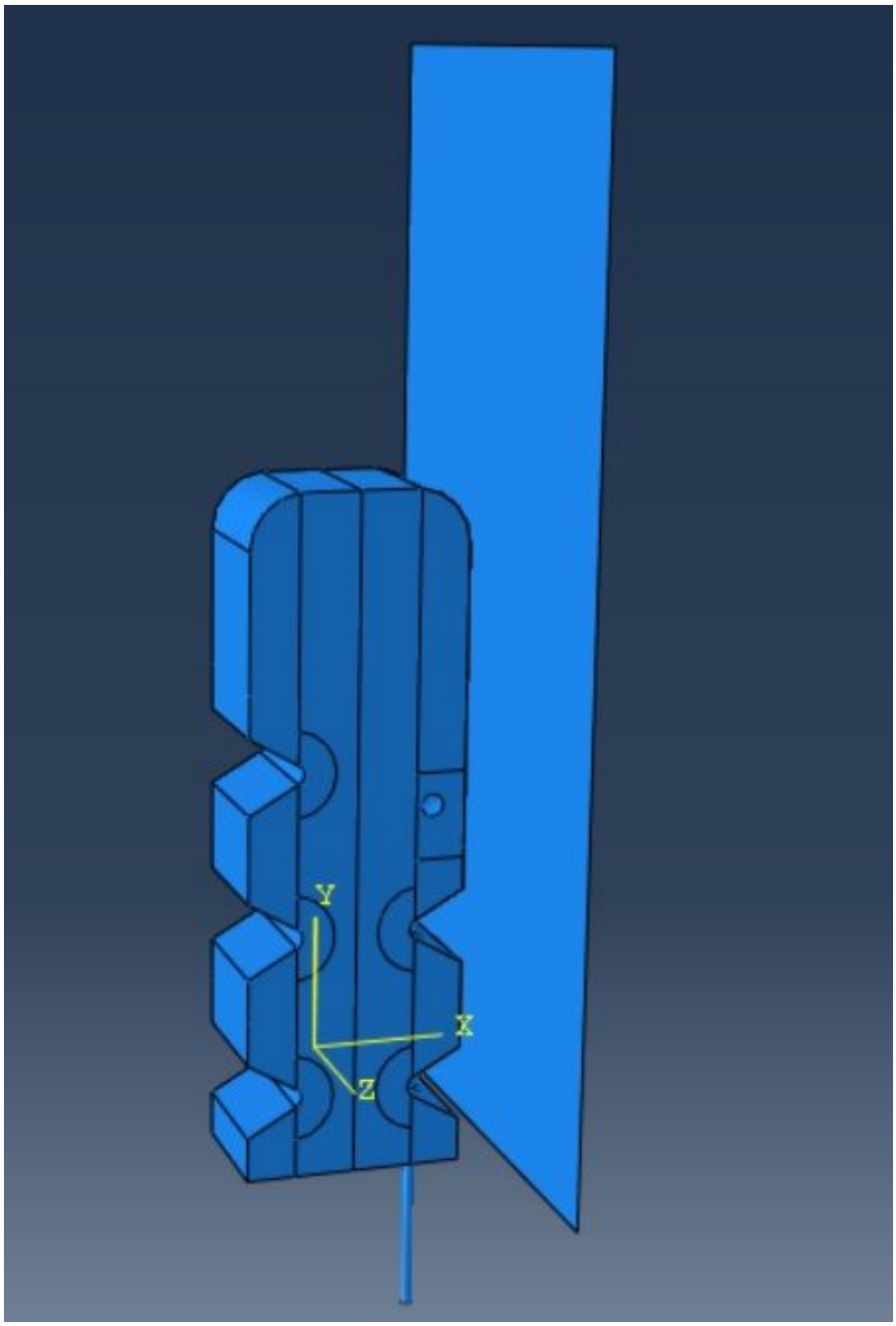

Figure 14

FE model for gripping simulation

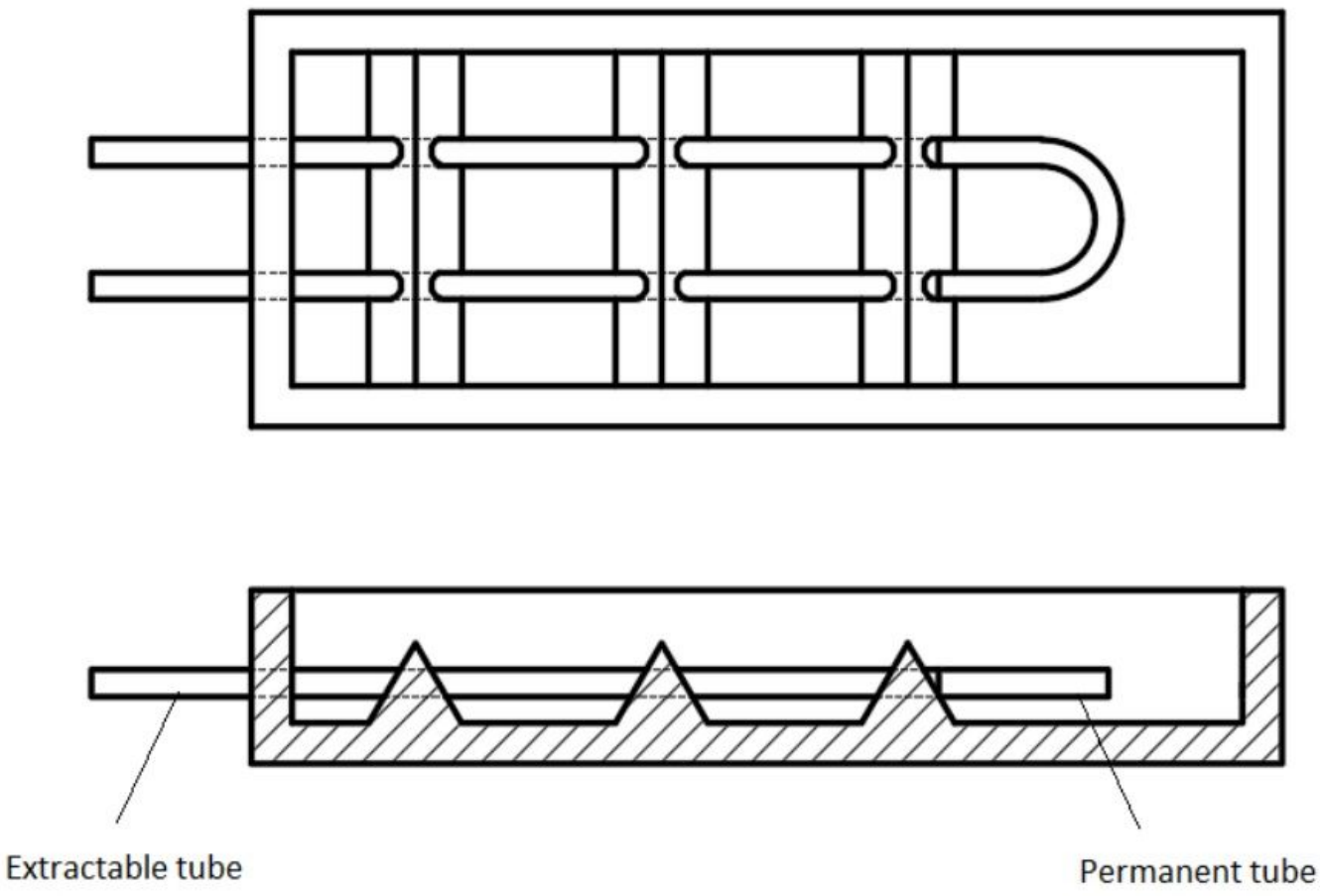

Figure 15

Overmolding illustration

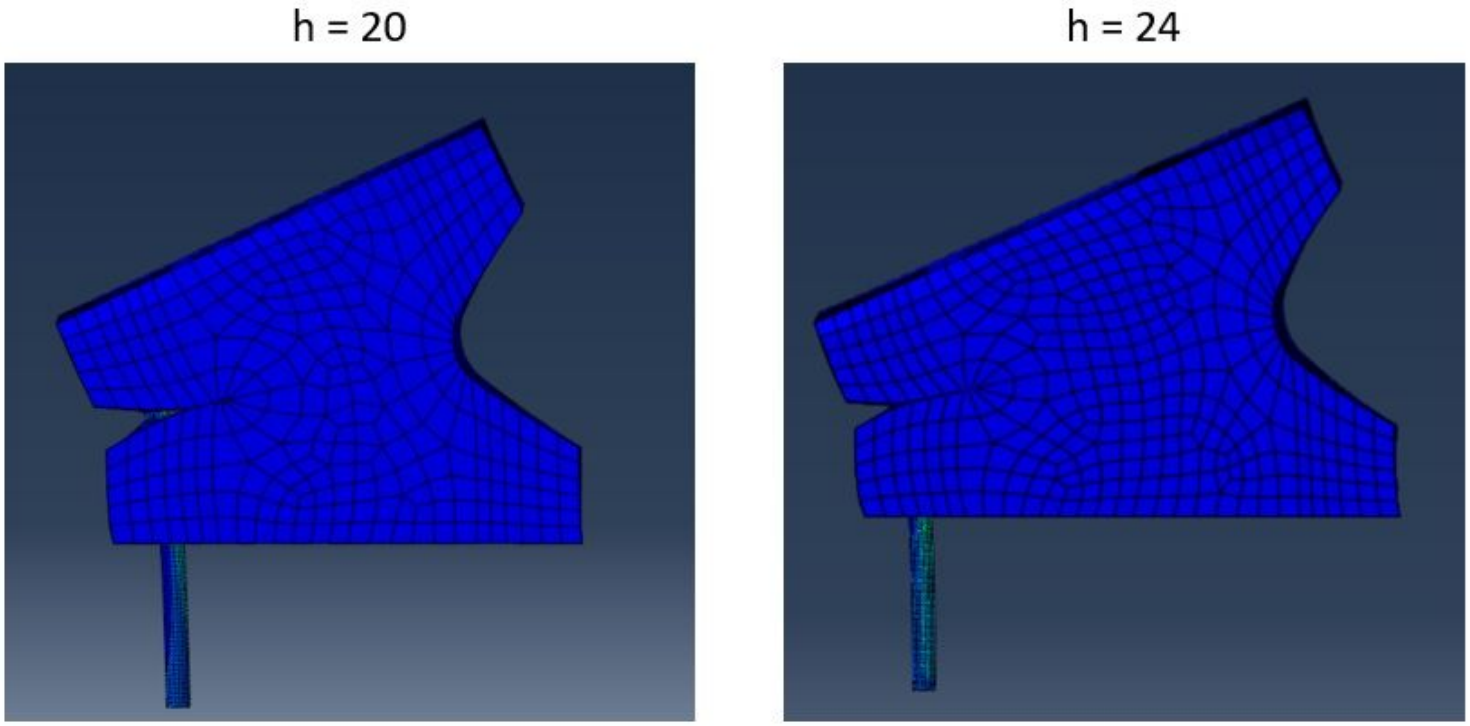

Figure 16

Sample results

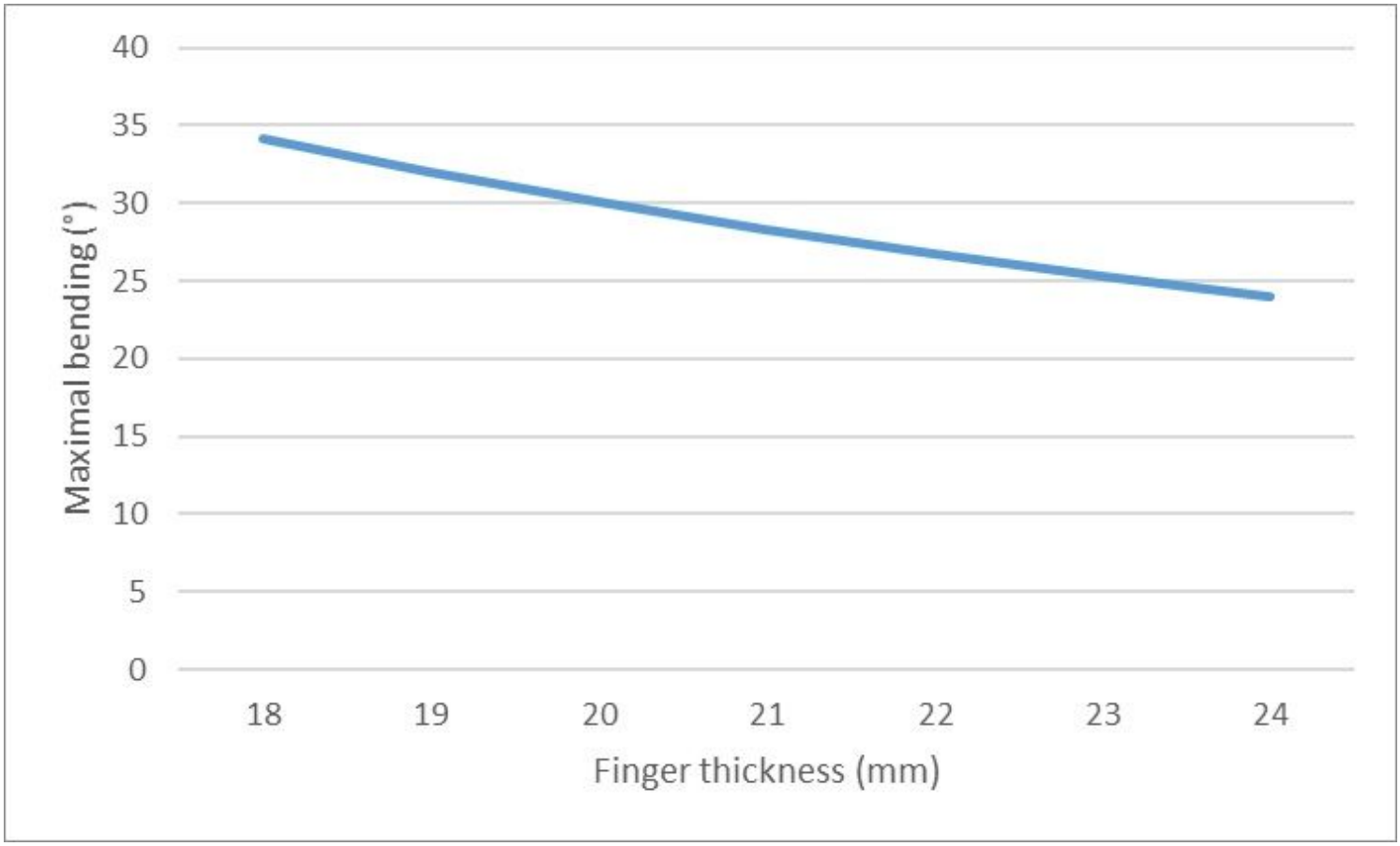

Figure 17

Maximal bending magnitude of different thickness

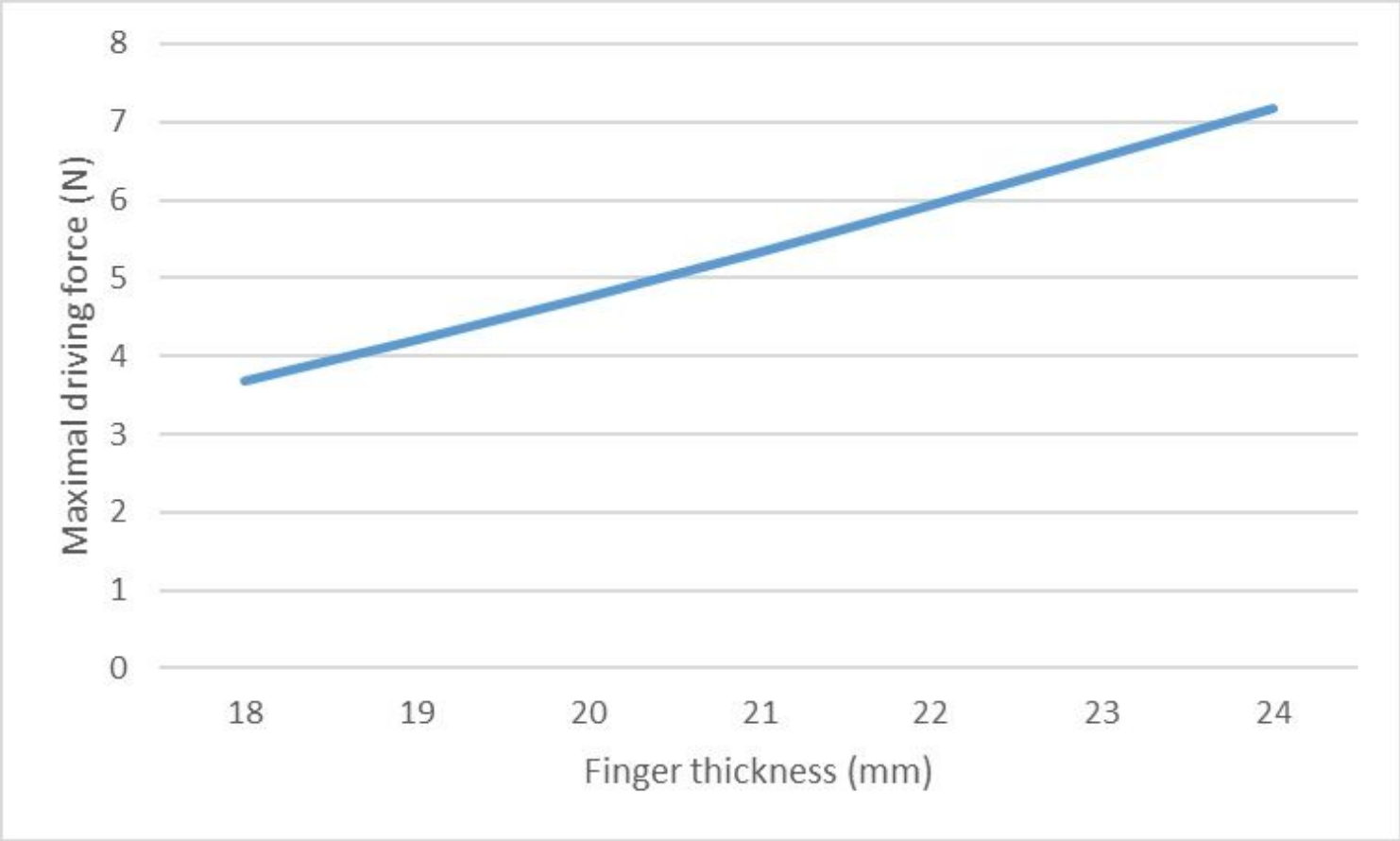

Figure 18

Maximal driving force for different thickness

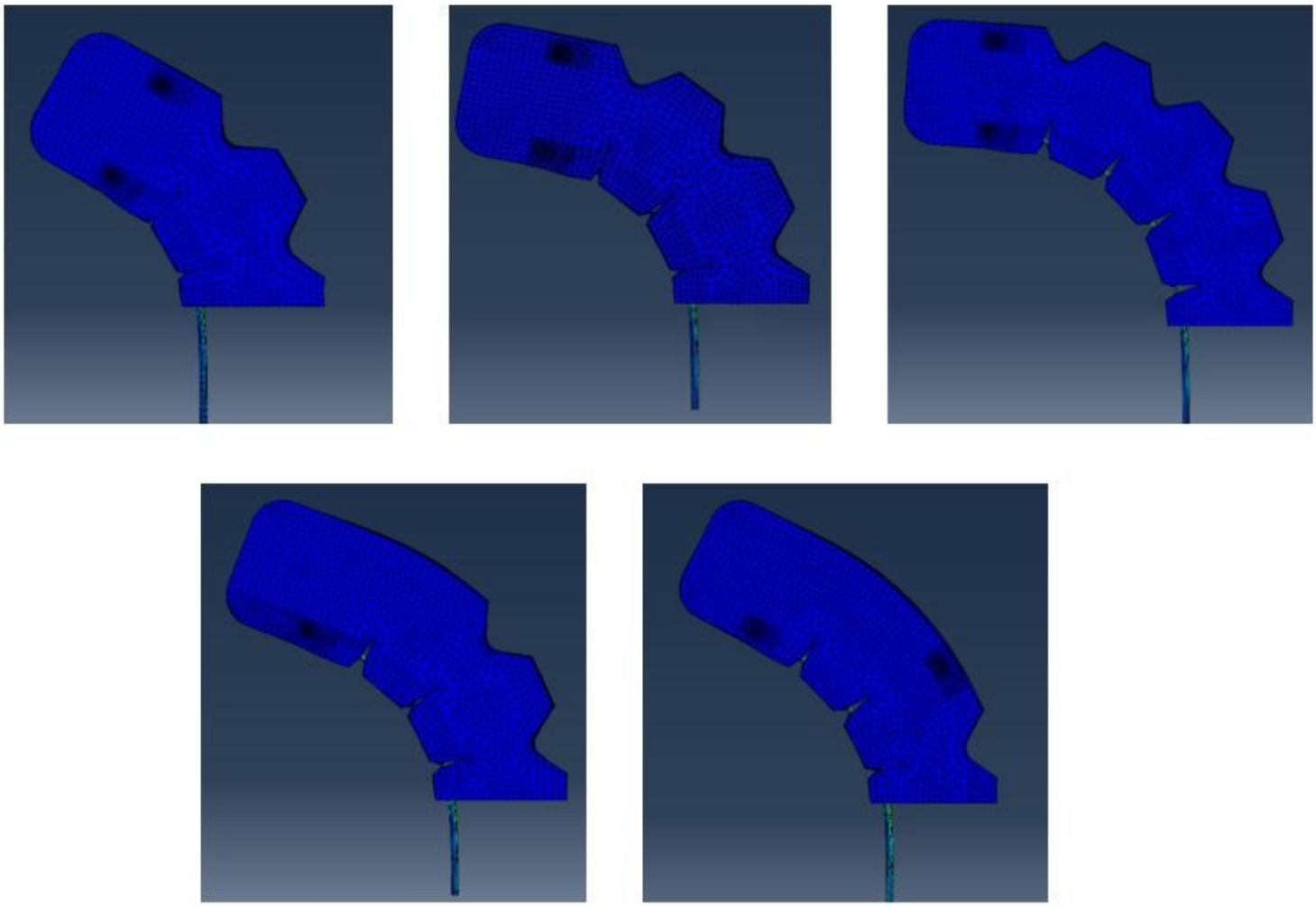

Figure 19

Deformation results of different configurations

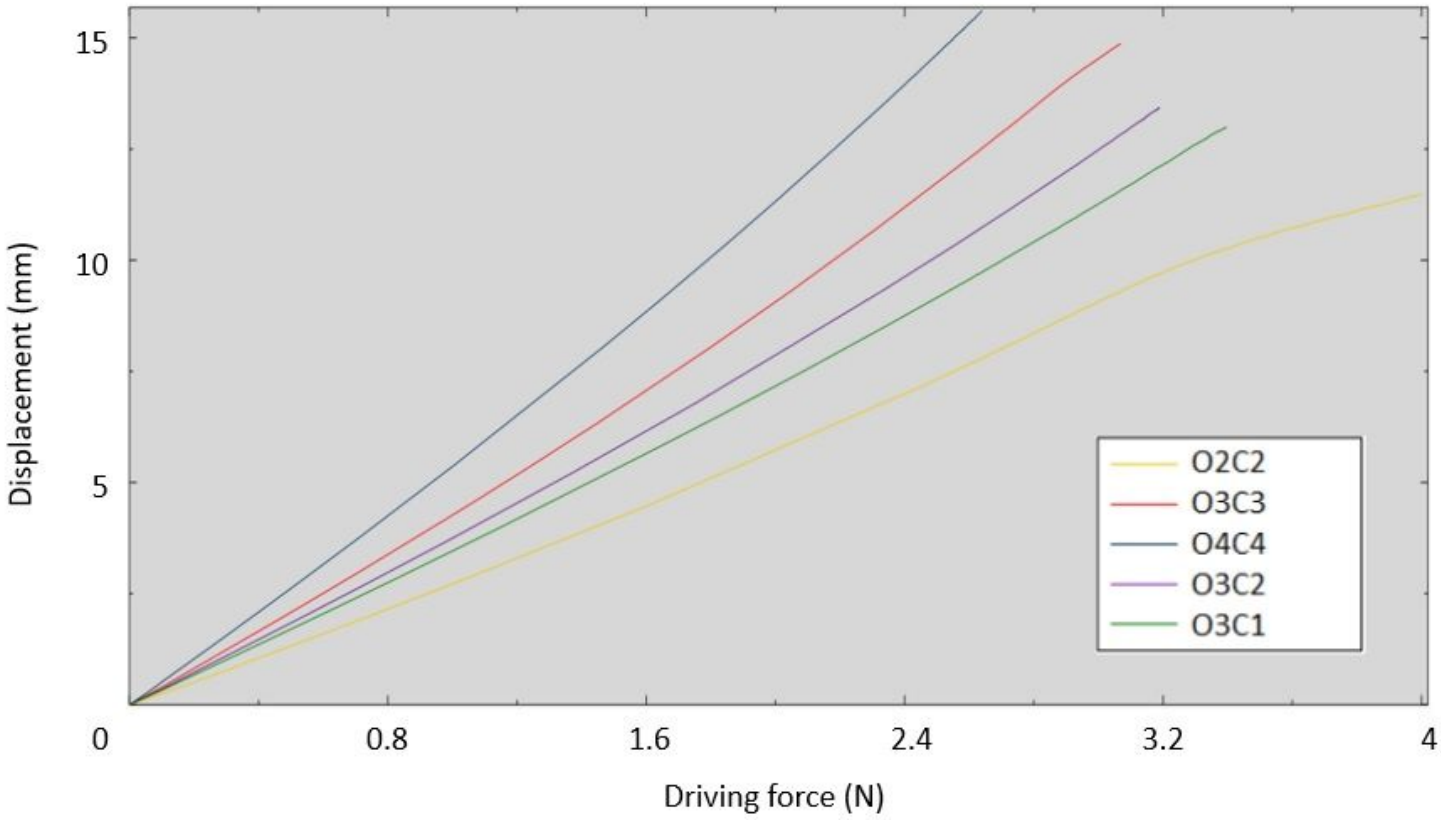

Figure 20

Displacement-force results of different configurations

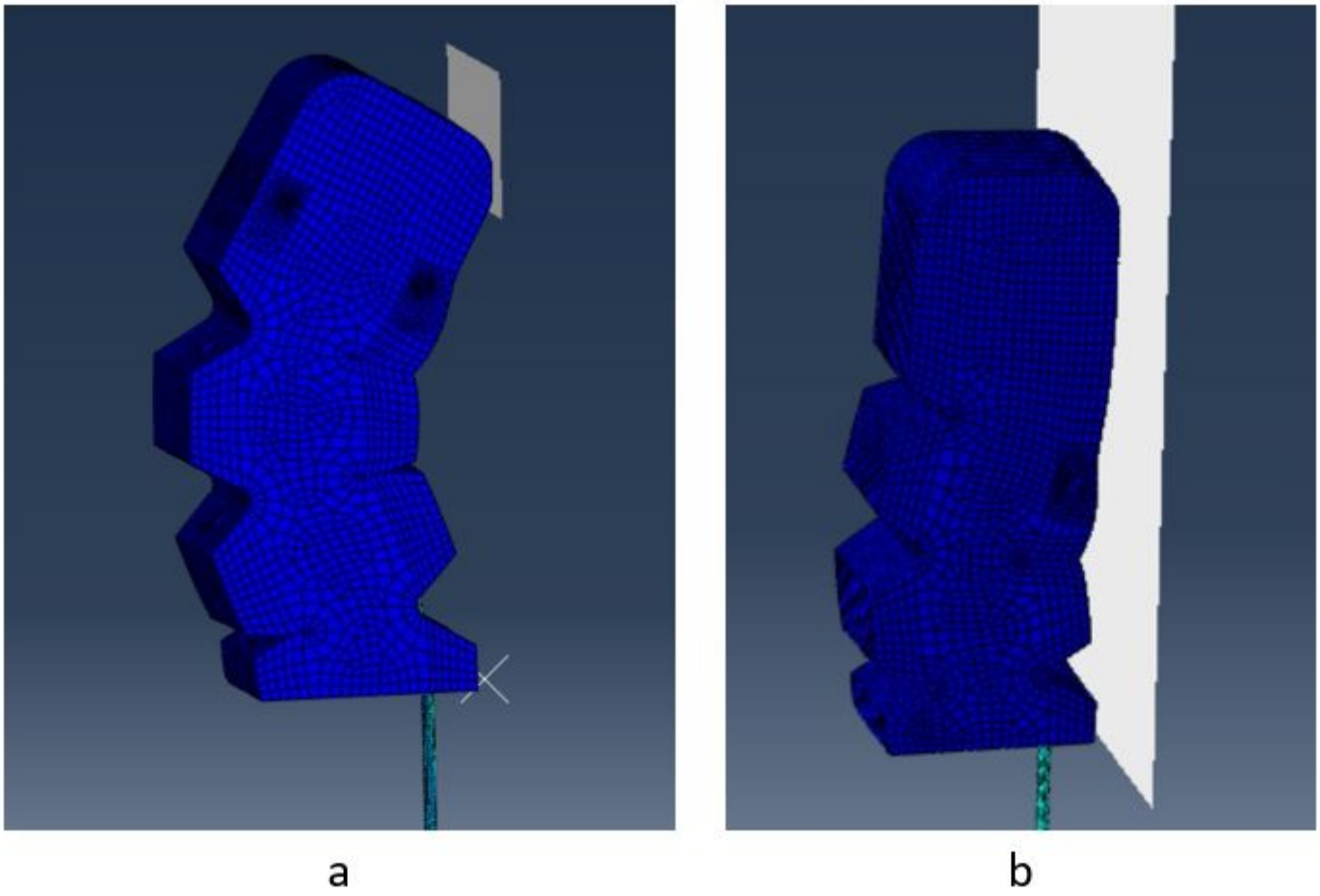

Figure 21

Different gripping conditions a. Rolling grip; b. Firm grip

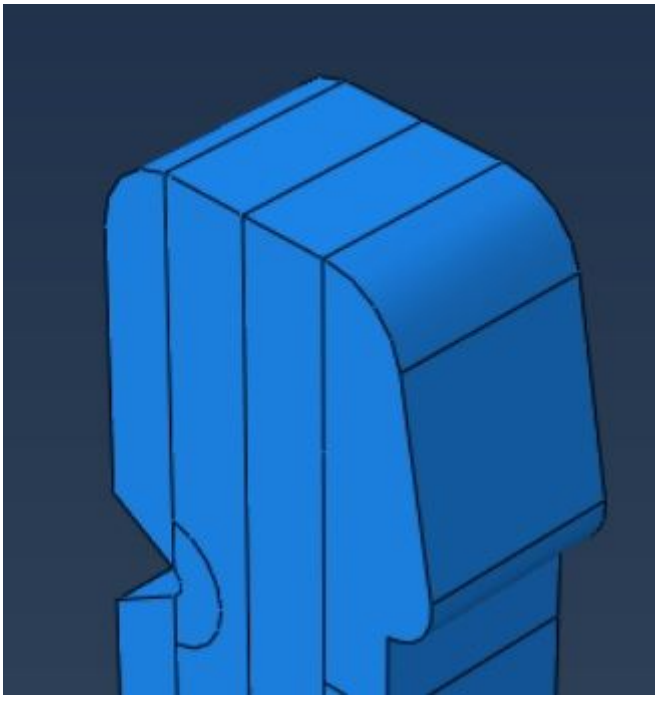

Figure 22

Inclined fingertip

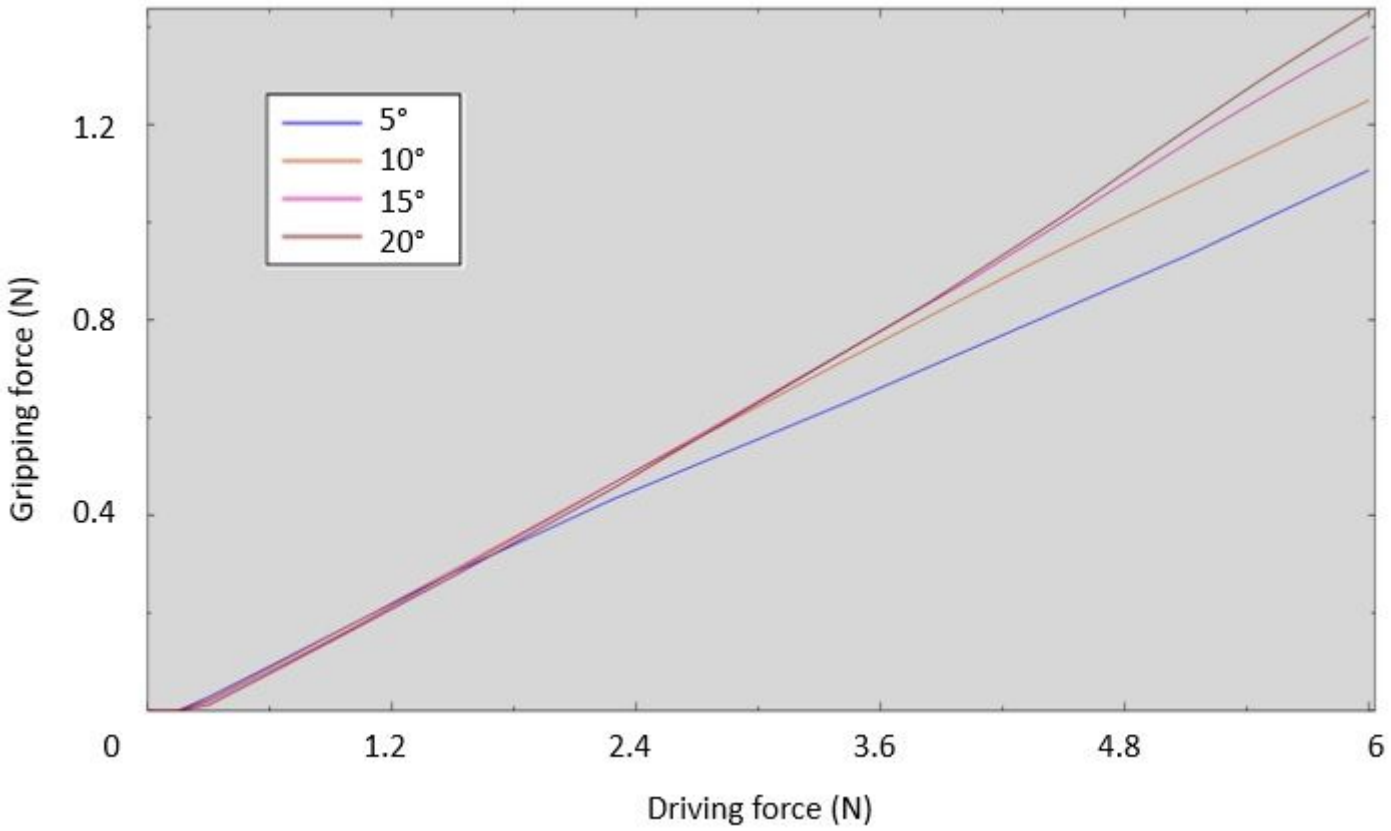

Figure 23

Gripping force of different fingertip angles

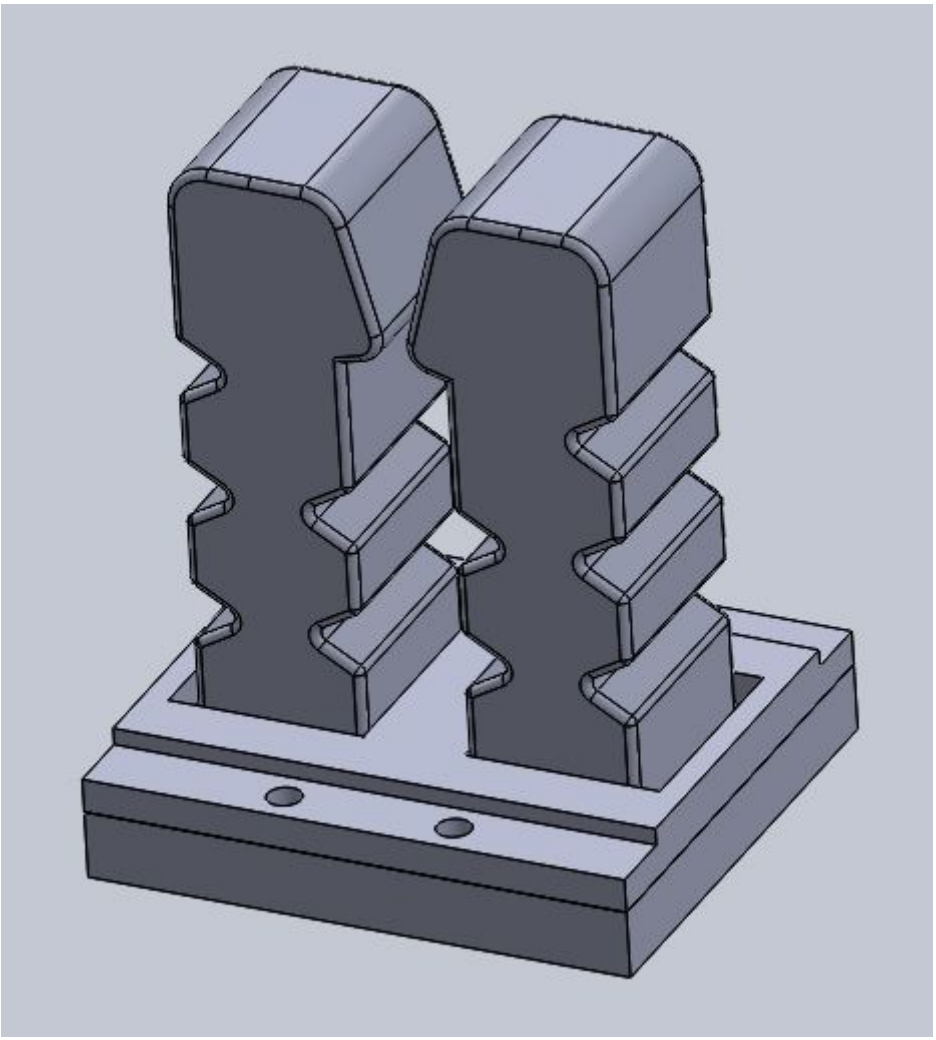

Figure 24

CAD model of the gripper

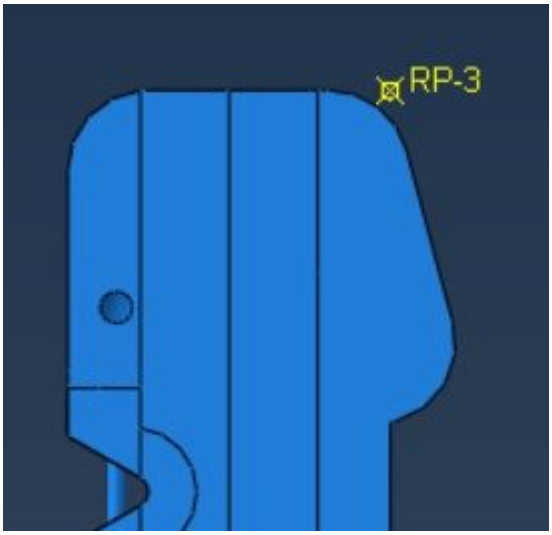

Figure 25

Fingertip reference point

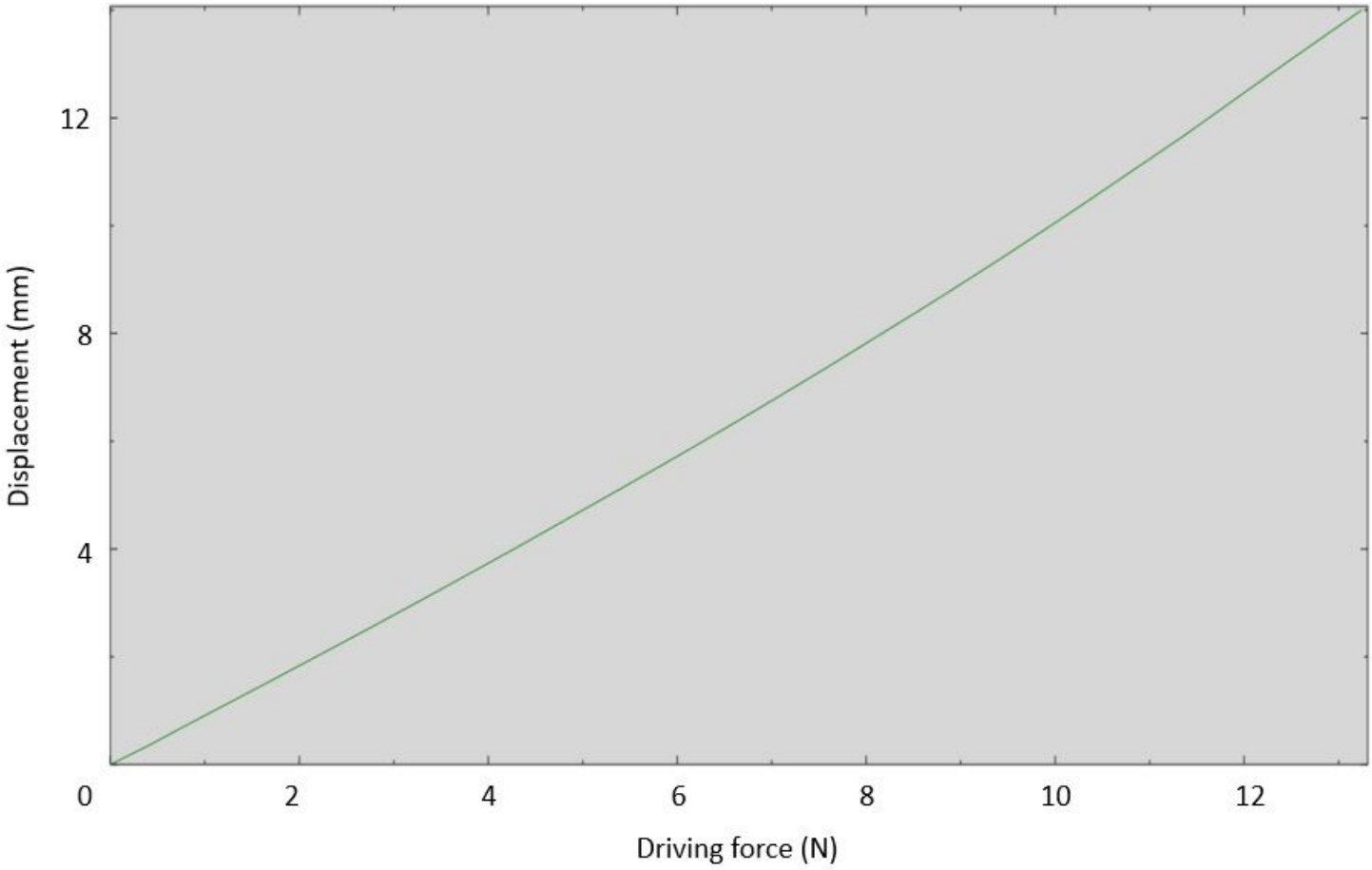

Figure 26

String tip displacement

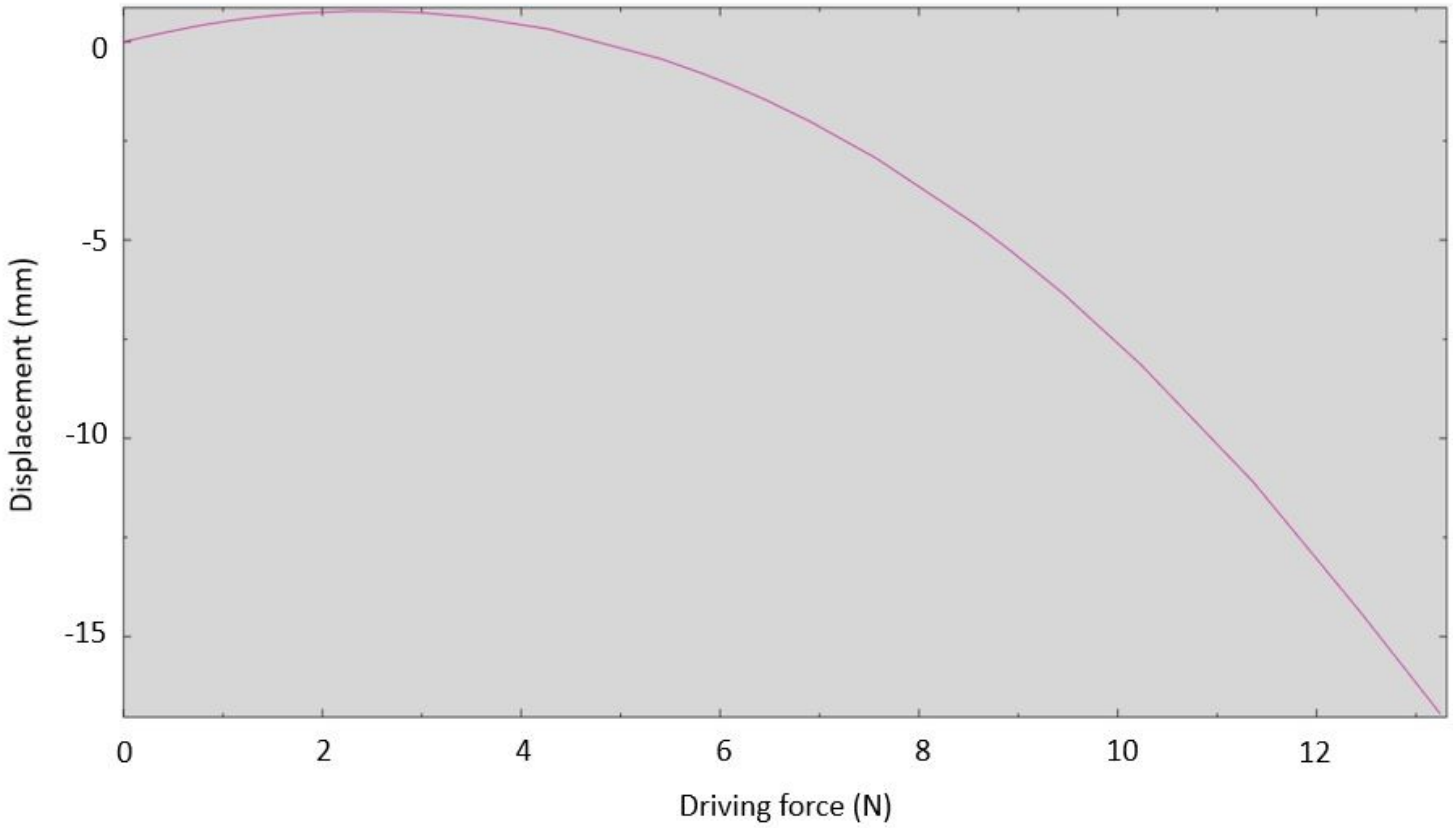

Figure 27

Fingertip displacement in vertical direction

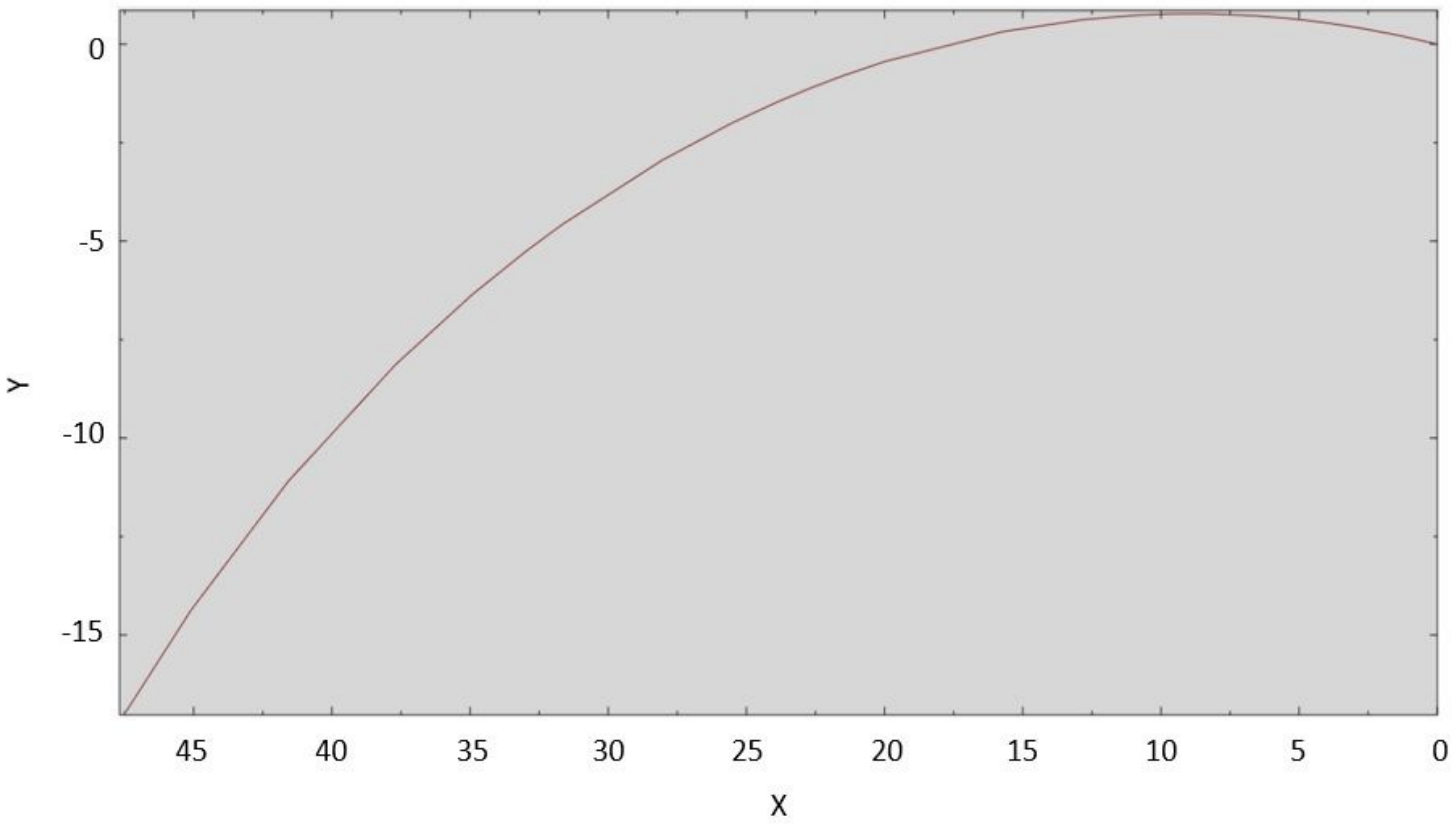

Figure 28

Fingertip trajectory

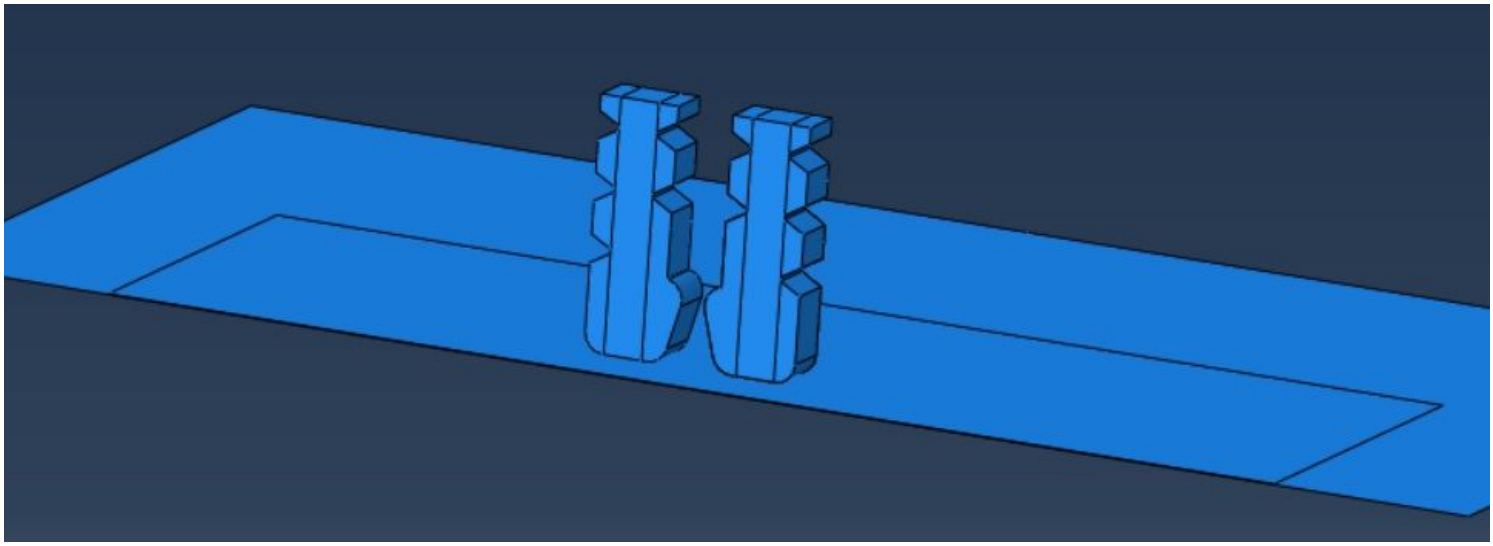

Figure 29

FE model for gripping simulation

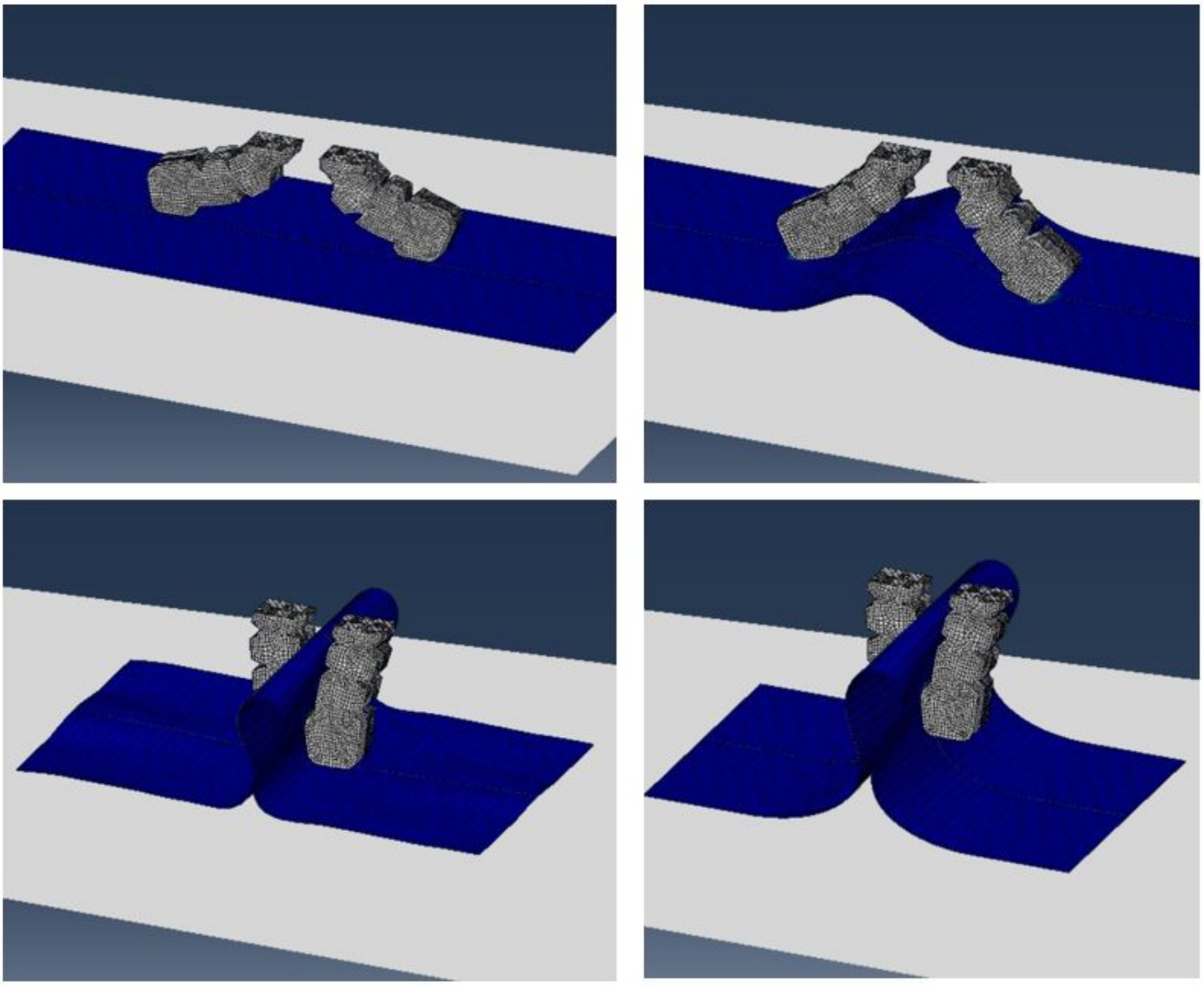

Figure 30

Gripping simulation

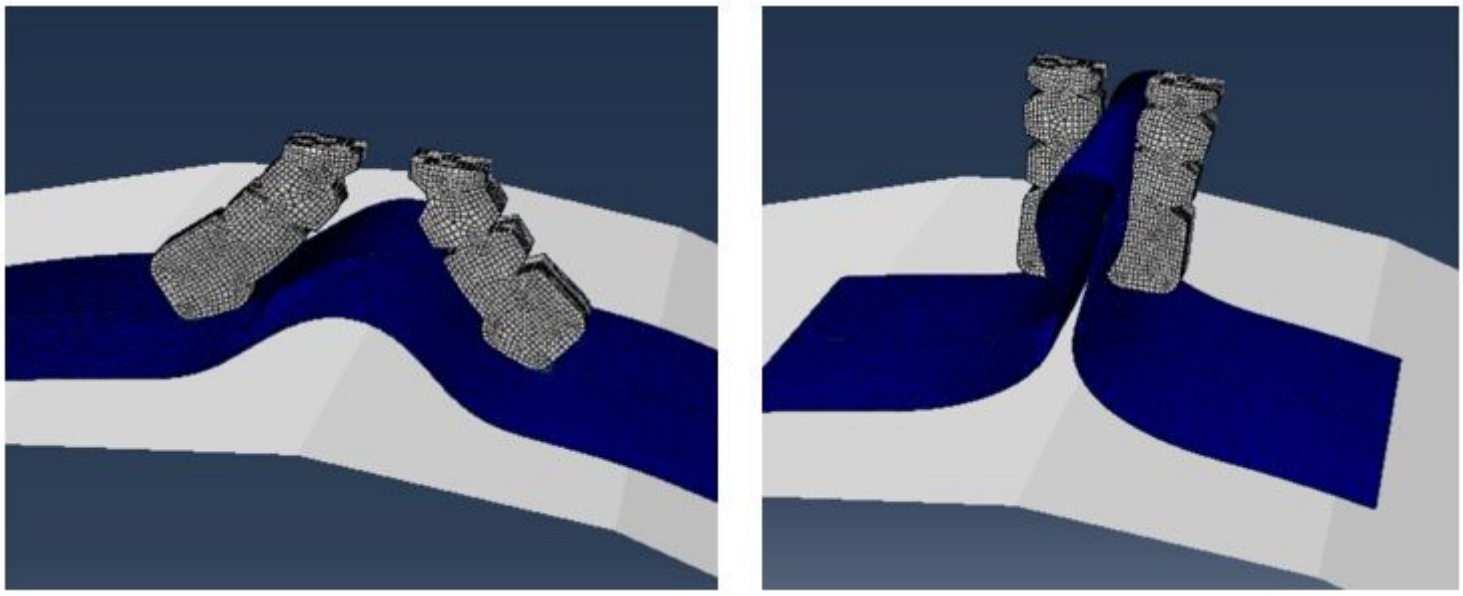

Figure 31

Gripping simulation on a curved surface

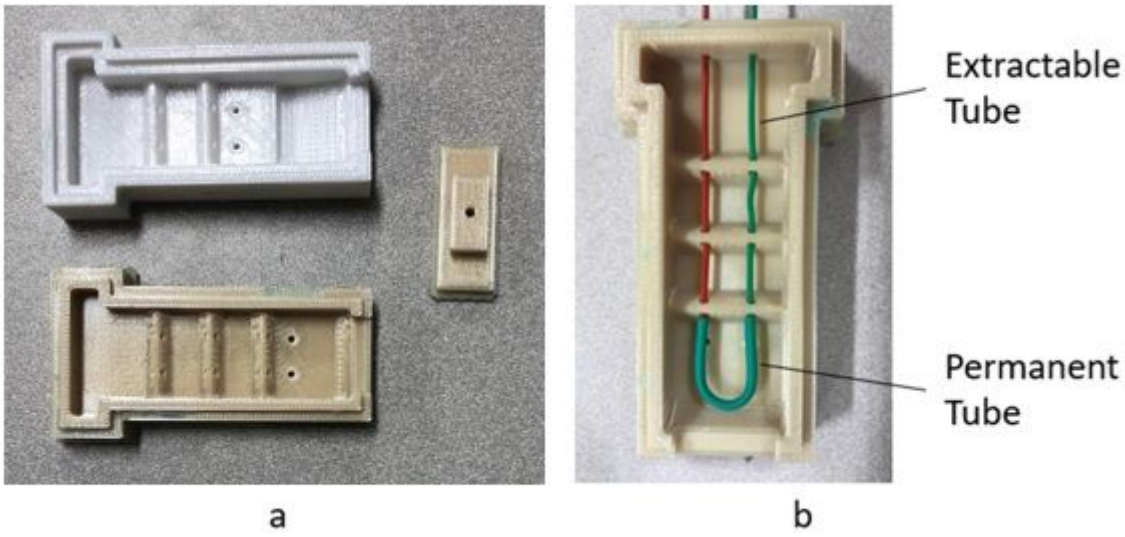

Figure 32

Mold set

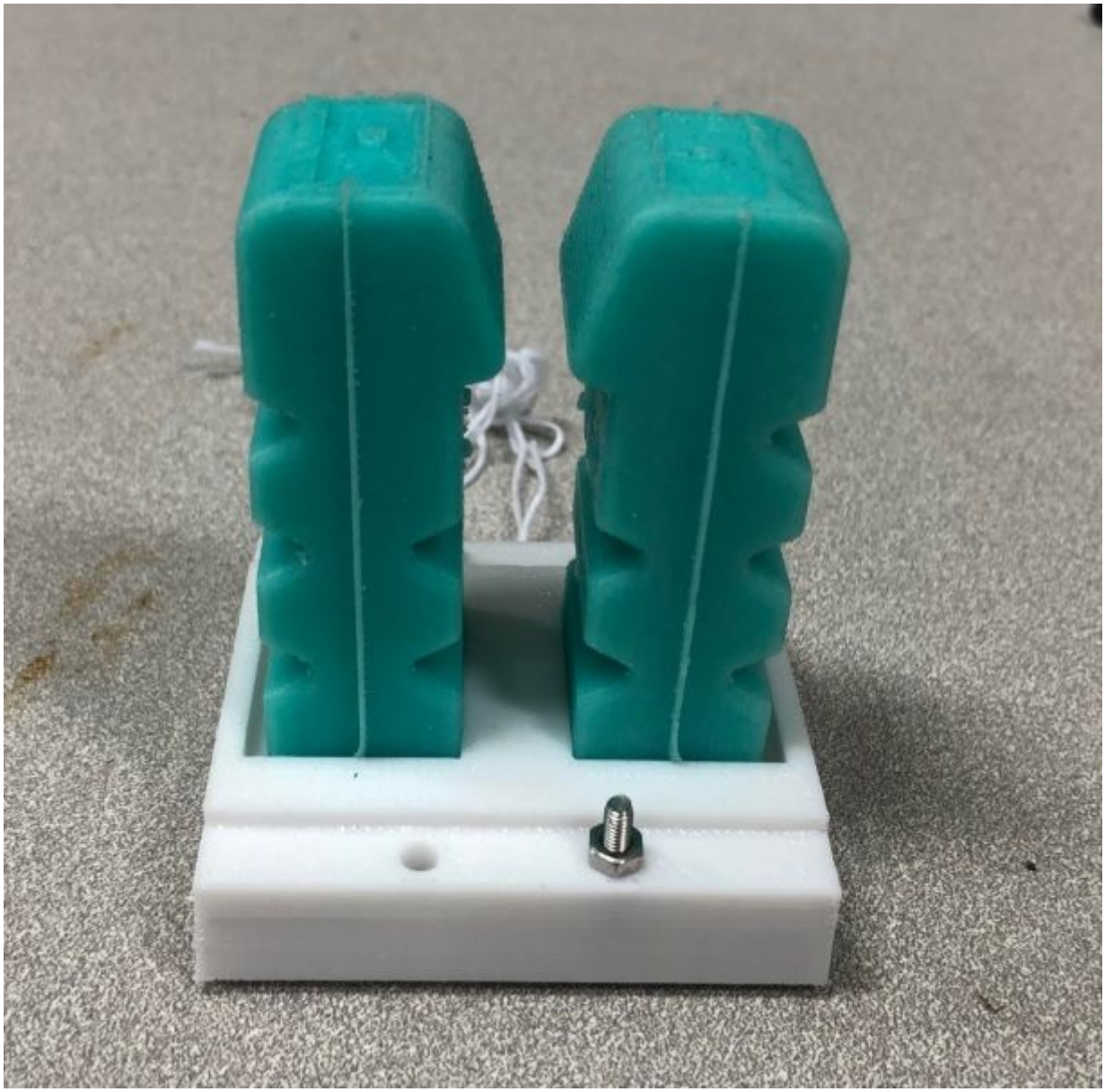

Figure 33

Gripper prototype

Figure 34

Manual tests a. Picking up a single ply; b. Separating a ply from a stack; c. De-wrinkling

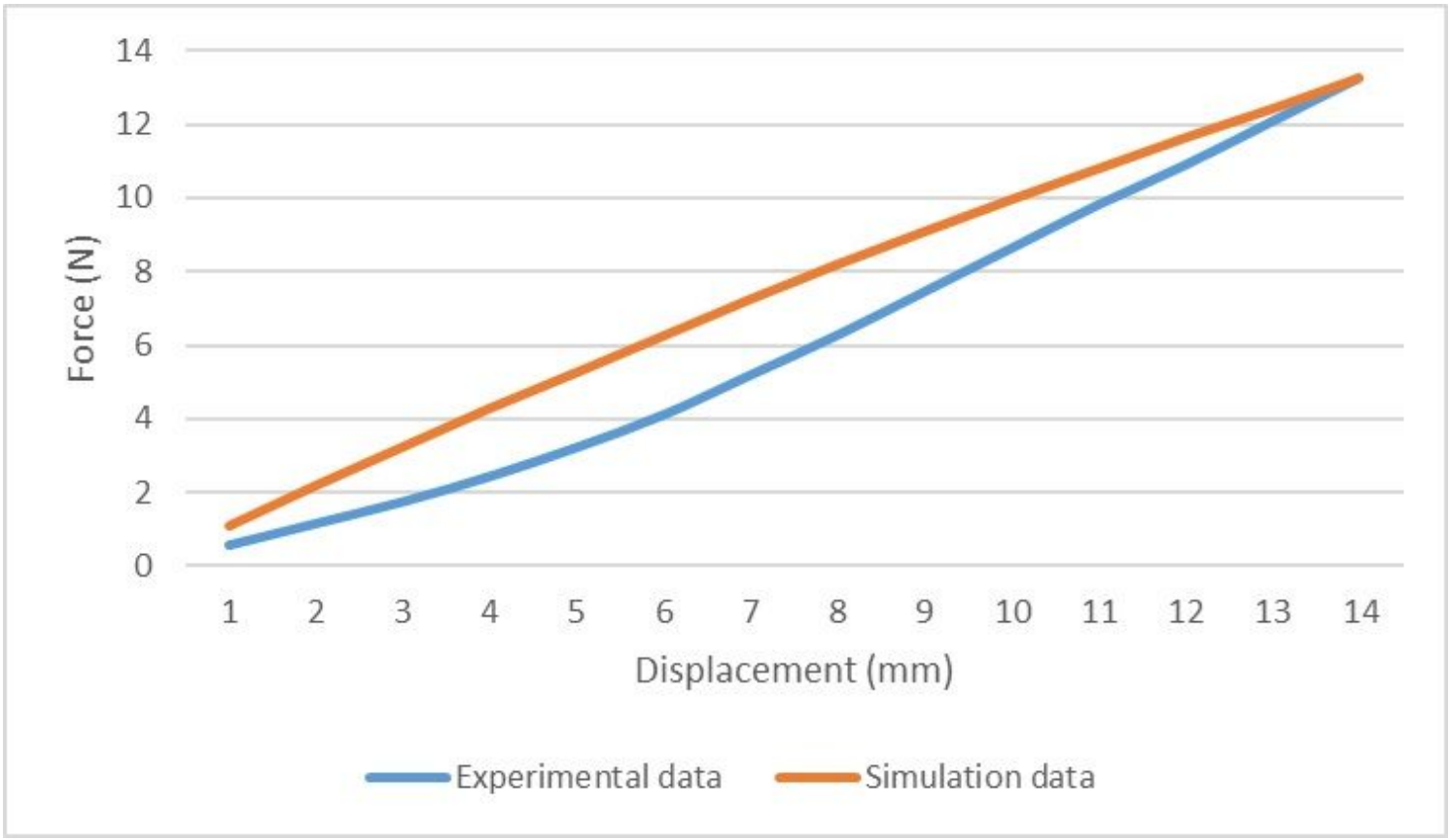

Figure 35

Comparison between experimental data and simulation data